Although there is a growing body of information reporting Mϕ activation by CpG DNA, most studies have been performed using Mϕ cell lines derived from the mouse. Few studies have been reported using primary cultured Mϕs freshly isolated from animals, which would be a better model than immortalized cells lines as far as reflecting the *in vivo* situation is concerned.

Previously we have demonstrated that Kupffer cells (liver-resident Mϕs) play an important role in the processing of pDNA after intravenous injection into mice.[18] *In vitro* experiments, using mouse peritoneal resident Mϕs, have also shown that primary cultured Mϕs take up pDNA efficiently via a scavenger receptor-like mechanism and in a specific manner.[19,20] In the present study, we evaluated Mϕ activation, following stimulation with naked pDNA, using mouse peritoneal resident and elicited cultured Mϕs in comparison with the Mϕ cell lines RAW264.7 and J774A1. We found that the peritoneal Mϕs showed very low or almost no secretion of inflammatory cytokines following stimulation with pDNA, in spite of extensive uptake of CpG DNA. These results contrast with our recent finding that peritoneal Mϕs and RAW264.7 cells show similar responsiveness to pDNA complexed with cationic liposomes.[21]

MATERIALS AND METHODS

Chemicals

RPMI-1640, Dulbecco's modified Eagle's minimal essential medium (DMEM), Hanks' balanced salt solution (HBSS) and thioglycolate broth were obtained from Nissui Pharmaceutical (Tokyo, Japan). Triton X-114 was purchased from Nacalai Tesque (Kyoto, Japan).

Cell cultures

Male ICR mice (5 weeks of age) were purchased from the Shizuoka Agricultural Cooperative Association for Laboratory Animals (Shizuoka, Japan). Resident Mϕs were collected (in RPMI-1640) from the peritoneal cavity of unstimulated mice. Cells were washed, suspended in RPMI-1640 supplemented with 10% fetal bovine serum (FBS), penicillin G (100 U/ml), streptomycin (100 μg/ml) and amphotericin B (1·2 μg/ml), and then plated on 24-well culture plates (Falcon; Becton Dickinson, Lincoln Park, NJ), at a density of 5×10^5 cells/well, for the cellular association experiments and activation experiments. For confocal microscopic observations, peritoneal cells were plated on a cover glass, in a 12-well culture plate, at a density of 5×10^5 cells/well. After a 2-hr incubation at 37° in 5% CO_2/95% air, adherent Mϕs were washed three times with RPMI-1640 to remove non-adherent cells and then cultured under the same conditions for 24 hr. For elicited Mϕs, all the processes were the same, except that 1 ml of 2·9% thioglycolate broth was injected intraperitoneally into mice 4 days prior to the collection of Mϕs. RAW264.7 or J774A1 cells were cultured in RPMI-1640 supplemented with 10% FBS, penicillin G (100 U/ml) and streptomycin (100 μg/ml). They were then plated on a 24-well culture plate at a density of $2·5 \times 10^5$ cells/ml and cultured for 24 hr.

Plasmid DNA

The vector pcDNA3 was purchased from Invitrogen (Carlsbad, CA). The vector pCMV-Luc, encoding the firefly luciferase gene, was constructed as described previously.[22] pcDNA3 contains 26 5′-Pur-Pur-CpG-Pyr-Pry-3′ sequences, including two GACGTT sequences which have been reported to be the most potent sequences for mice.[7] For the cellular-association experiment, pCMV-Luc was radiolabelled with [α-^{32}P]dCTP by nick translation.[23] The reaction was performed on 1 μg of pDNA (pCMV-Luc) in a final volume of 40 μl. The incubation buffer was 50 mM Tris–HCl, pH 7·8, 10 mM $MgCl_2$, 0·1 mM dithiothreitol (DTT) and 0·0025% bovine serum albumin (BSA). The reaction was initiated by adding 4 U of *Escherichia coli* (*E. coli*) DNA Polymerase I (Takara, Kyoto, Japan) and 0·0004 U of DNAse I (Takara) in the presence of 40 nM unlabelled triphosphate (dATP, dGTP, dTTP) and [α-^{32}P]dCTP (3·7 MBq, 100 μCi). After a 2-hr incubation at 15°, the reaction was terminated by heating at 70° for 10 min. Unincorporated nucleotides were removed using a Sephadex G-50 column. For the confocal microscopy study, pCMV-Luc was labelled using a Fasttag Texas Red labelling kit, according to the manufacturer's instructions (Vector Laboratories, Burlinghame, CA).

Purification of pDNA

To minimize any activation as a result of contaminating lipopolysaccharide (LPS), we used DNA samples extensively purified with Triton X-114, a non-ionic detergent. Extraction of endotoxin from pDNA, methylated-CpG pDNA, *E. coli* DNA and calf thymus DNA samples was performed according to previously published methods,[24,25] with slight modifications. DNA samples were purified by extraction with phenol–chloroform–isoamyl alcohol (25 : 24 : 1; v/v/v) and ethanol precipitation. Ten micrograms of DNA was diluted with 20 ml of pyrogen-free water, then 200 μl of Triton X-114 was added, followed by mixing. The solution was placed on ice for 15 min and then incubated for 15 min at 55°. Subsequently, the solution was centrifuged (20 min, 25°, 600 *g*). The upper phase was transferred to a new tube, 200 μl of Triton X-114 was added and the previous steps were repeated three or more times. The activity of LPS was measured by the Limulus amebocyte lysate (LAL) assay using the Limulus F Single Test kit (Wako, Tokyo, Japan). After purification using the Endo-free™ plasmid Giga kit, 1 μg/ml pDNA was found to contain 0·01–0·05 endotoxin units (EU)/ml. After extraction using Triton X-114, the endotoxin levels of DNA samples could no longer be determined by the LAL assay, i.e. 1 μg/ml DNA contained less than 0·001 EU/ml. Without extraction of endotoxin by Triton X-114, 100 μg/ml naked pDNA, containing 1–5 EU/ml, was able to stimulate the release of 521 ± 73 pg/ml TNF-α at 24 hr.

ODN

Phosphorothioate ODN was purchased from GENSET (Paris, France). The sequence of CpG S-ODN 1668 (a proven activator of murine immune cells, as previously described) is 5′-TCCATGACGTTCCTGATGCT-3′.[5,26] Phosphorothioate non-CpG ODN 1720 (5′-TCCATGAGCTTCCTGATGCT-3′) was used as a control. CG motifs and control GC sequences are underlined. Fluorescein isothiocyanate (FITC)-labelled CpG ODN was purchased from Sawady Technology (Tokyo, Japan).

Reverse transcription–polymerase chain reaction (RT–PCR)

Total RNA was extracted from cells using TRIzol (Invitrogen). Five micrograms of RNA was reverse-transcribed to complementary

DNA using the SUPERSCRIPT First-Strand Synthesis System for RT–PCR (Invitrogen). Fragments were amplified with *Taq* polymerase (Takara) using the following primer pairs: mTLR-9, 5′-CCGCAAGACTCTATTTGTGCTGG-3′ and 5′-TGTCCCTAGTCAGGGCTGTACTCAG-3′,[15] and glyceraldehyde-3-phosphate dehydrogenase (GAPDH), 5′-TCACCATCTTCCAGGAGCGA-3′ and 5′-ACCAGGAAATGAGCTTGACA-3′. The PCR temperature and cycles were as follows: 60 seconds at 95°, 90 seconds at 56° and 30 seconds at 72°, for 30 cycles. The size of the mTLR-9 and GAPDH products were 260 bp and 720 bp, respectively.

For the fragmentation or denaturation of DNA, pDNA were diluted in endotoxin-free water, to a concentration of 1 mg/ml in a 0·5 ml tube, and sonicated for 2 hr in an ultrasonic automatic washer (Iuchi, Tokyo, Japan). Separately, DNA was heat-denatured at 95° for 10 min. DNA was incubated at 4° before use.

Cytokine secretion

Mouse Mϕs, resident and elicited peritoneal Mϕs from ICR mice, and the Mϕ cell lines, RAW264.7 and J774A1, were washed three times with 0·5 ml of RPMI-1640 before use. Naked DNA was diluted in 0·5 ml of Opti-MEM and the cells were incubated for 8 hr with this solution. Then, the cells were washed with RPMI-1640 and incubated with RPMI-1640 containing 10% FBS, continuously, for specified time-periods of up to 48 hr. In the inhibition experiments, cells were incubated with the medium containing an inhibitor alone, at various concentrations, for 30 min, then incubated with the medium containing DNA or liposome formulations together with the inhibitor. At the indicated time-points, the supernatants were collected for enzyme-linked immunosorbent assay (ELISA) and stored at −80°. The levels of TNF-α and IL-6 in the supernatants were determined by using the OptEIA™ set (Pharmingen, San Diego, CA). The detection limit of these sets was 15·6 pg/ml for both cytokines.

Cellular-association experiments

Mouse peritoneal Mϕs and RAW264.7 cells were cultured in 24-well plates. The cells were washed twice with HBSS (without phenol red) and then incubated, at 37°, with HBSS containing trypsin (50 μg/ml). Then, the cells were washed with HBSS and incubated with HBSS containing ^{32}P-labelled pDNA (0·1 μg/ml). After a 3-hr incubation at 4°, the cells were washed three times with ice-cold HBSS and then solubilized with 1·0 ml of 0·3 N NaOH containing 0·1% Triton-X-100. Aliquots were taken for the determination of ^{32}P radioactivity using an LSA-500 scintillation counter (Beckman, Tokyo, Japan). The protein content was measured using the modified Lowry method[27] with BSA as a standard.

Trichloroacetic acid (TCA) precipitation experiments

After the cellular-association experiments, the medium and cell lysate containing radioactivity derived from ^{32}P-labelled pDNA were subjected to TCA-precipitation experiments to assess the degradation of pDNA by Mϕs. A portion of the cell lysate was directly subjected to radioactivity counting and the protein content was measured as described above. The cell lysis solution was neutralized with 1 N HCl, and the same volume of 10 mM Tris-HCl, 1 mM EDTA (TE)-saturated phenol (pH 7·8) was added. The mixture was vortexed and centrifuged at 13 500 *g* for 10 min. The upper phase was transferred to another tube to which the same volume of ice-cold 10% TCA was added, and the tube was vortexed. After a 10-min incubation on ice, the solution was centrifuged at 13 500 *g* for 25 min. Supernatants were used for the determination of radioactivity. To quantify the amount of free [α-^{32}P]dCTP in ^{32}P-labelled pDNA, TCA precipitation of a standard sample was performed.

Confocal microscopy

Cells were washed three times with 1·0 ml of HBSS and then incubated, in HBSS, at 4° for 10 min. The cells were then incubated with HBSS containing Texas Red-labelled pDNA and FITC-labelled CpG S-ODN at 4° for 30 min. The cells were washed five times with HBSS and incubated at 37° for 15 min. Then, the cells were fixed with 4% paraformaldehyde for 10 min. The cells were scanned by confocal microscopy (MRC-1024; Bio-Rad, Hercules, CA).

RESULTS

Peritoneal Mϕs do not secrete inflammatory cytokines upon stimulation with naked pDNA

Secretion of inflammatory cytokines, induced by CpG DNA, was examined using mouse Mϕ cell lines and peritoneal Mϕs. *E. coli* DNA and pDNA were models of CpG DNA, and calf thymus DNA was used as non-CpG DNA. DNA was extensively purified with phenol and Triton X-114 to avoid contamination with LPS and some bacterial proteins. Two different cell lines – RAW264.7 and J774A1 – secreted a large amount of TNF-α, upon stimulation with naked *E. coli* DNA and pDNA, in a concentration-dependent manner (Fig. 1). Calf thymus DNA was unable to induce the secretion of TNF-α. Digested *E. coli* DNA was unable to stimulate the secretion of TNF-α from RAW264.7 cells. These results indicated that, similarly to ODN, naked DNA also activates these Mϕ cell lines to produce inflammatory cytokines in a CpG motif-dependent manner. Similar experiments were carried out using two types of mouse peritoneal Mϕs – resident and elicited Mϕs – isolated from male ICR mice. Surprisingly, CpG DNA, pDNA and *E. coli* DNA were unable to induce TNF-α release from either resident or elicited Mϕs in primary culture, even at a high concentration (100 μg/ml DNA) for up to 24 hr (Fig. 2). Another inflammatory cytokine, IL-6, also failed to be detected in resident Mϕs. LPS stimulated all types of Mϕs to secrete TNF-α.

Expression of TLR-9 mRNA and cytokine release induced by CpG DNA from peritoneal Mϕs and RAW264.7 cells

TLR-9 recognizes bacterial CpG motifs. To confirm the reactivity of peritoneal Mϕs with CpG DNA, we tested the mRNA expression of TLR-9 in these cells by RT–PCR. Both resident peritoneal Mϕs and RAW264.7 cells showed TLR-9 mRNA expression (Fig. 3). Moreover, CpG ODN 1668 was able to induce TNF-α from the resident Mϕs (Fig. 4a). CpG DNA requires endocytosis and endosomal acidification to induce inflammatory responses.[26,28,29] It was shown that endosomal

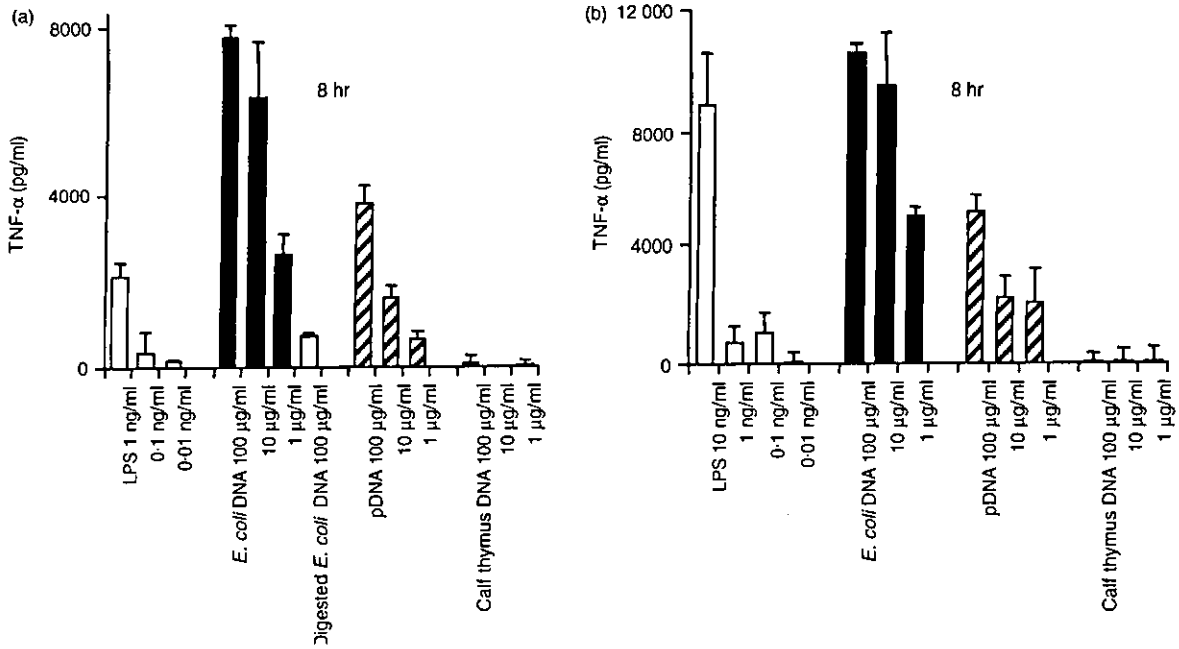

Figure 1. Cytokine release induced by naked plasmid DNA (pDNA) or other DNAs from macrophage (Mϕ) cell lines. RAW264.7 cells (a) or J774A1 cells (b) were incubated with lipopolysaccharide (LPS) (white bar), *Escherichia coli* (*E. coli*) DNA (black bar), pDNA (hatched bar), or calf thymus DNA (shaded bar) for 8 or 24 hr. The amount of cytokines released from the Mϕs was quantified by enzyme-linked immunosorbent assay (ELISA). The concentration of cytokines present in medium only was subtracted from the cytokine concentration in each sample. Each result represents the mean and standard deviation (n = 3).

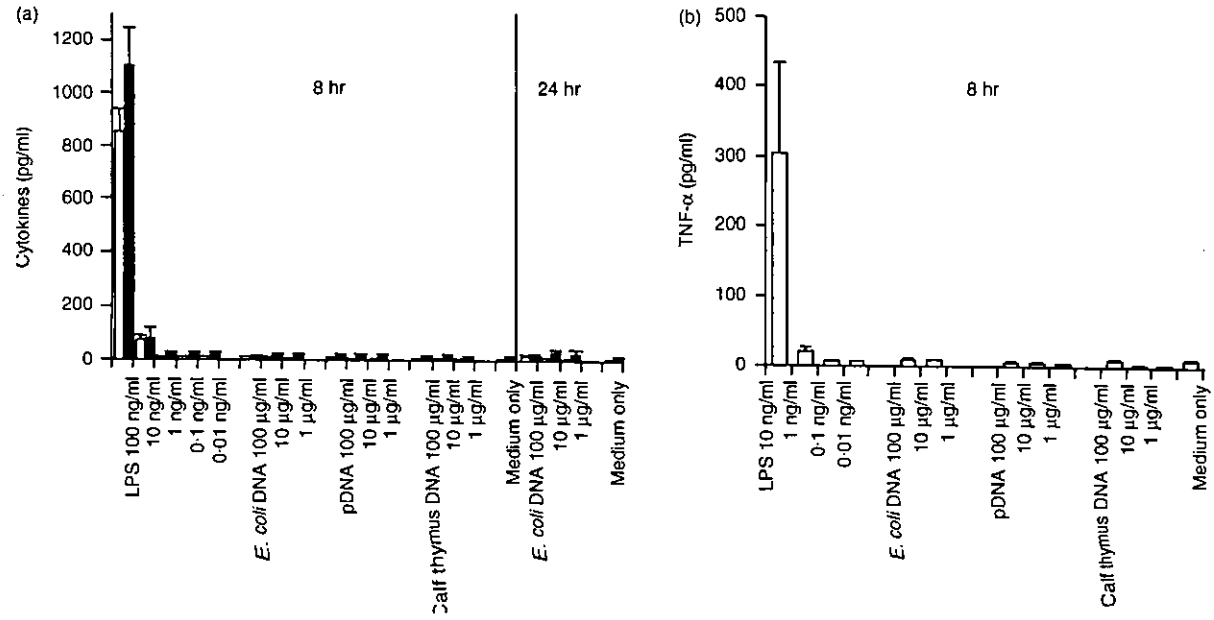

Figure 2. Cytokine release induced by naked plasmid DNA (pDNA) or other DNAs from primary cultured macrophages (Mϕs). Resident Mϕs (a) or elicited Mϕs (b) were incubated with lipopolysaccharide (LPS), *Escherichia coli* (*E. coli*) DNA, pDNA, or calf thymus DNA for 8 or 24 hr. The amount of tumour necrosis factor-α (TNF-α) (white bars) and interleukin-6 (IL-6) (black bars) released from the Mϕs was quantified by enzyme-linked immunosorbent assay (ELISA). Each result represents the mean and standard deviation (n = 3).

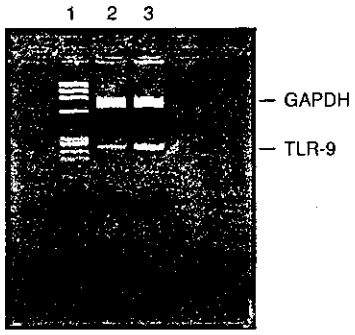

Figure 3. Expression of Toll-like receptor-9 (TLR-9) mRNA in macrophages (Mϕs). Total RNA was extracted from resident Mϕs or RAW264.7 cells. mRNA expression of TLR-9 was determined by reverse transcription–polymerase chain reaction (RT–PCR). DNA mobility was analysed by agarose-gel electrophoresis (3·5% gel). Lane 1, Φ-*Hae*III marker; lane 2, resident Mϕs; lane 3, RAW264.7 cells. GAPDH, glyceraldehyde-3-phosphate dehydrogenase.

acidification inhibitors, such as bafilomycin A, chloroquine or monensin, inhibited cytokine secretion by CpG ODN from RAW264.7 cells.[28] Therefore, the effect of these inhibitors on cytokine release from resident Mϕs was examined. The endocytosis inhibitor, cytochalasin B, inhibited the induction of TNF-α by CpG ODN from the resident Mϕs. TNF-α secretion was also significantly reduced by these endosomal acidification inhibitors.

In contrast to primary cultured Mϕs, RAW264.7 cells and J774A1 cells could be stimulated by pDNA to produce TNF-α (Fig. 1). The effect of inhibitors of endocytosis or endosomal acidification on the cytokine responses induced in RAW264.7 cells was examined. Cytochalasin B inhibited the TNF-α release that was stimulated by pDNA. Monensin, bafilomycin A and chloroquine, inhibitors of endosomal acidification, suppressed the induction of TNF-α (Fig. 4), suggesting that similar mechanisms are involved in cytokine induction by pDNA in Mϕs.

Cellular uptake and subsequent degradation of pDNA are not major factors in the unresponsiveness of peritoneal Mϕs to pDNA

It has been reported that TLR-9 is an intracellular protein.[30] To determine whether the difference in activation induced by CpG DNA (other than CpG S-ODN) is the result of a difference in the cellular uptake of DNA, we compared the degree of binding and uptake of ^{32}P-labelled pDNA in all the Mϕ types used in this study. The cellular association of ^{32}P-labelled pDNA in the RAW264.7 and J774A1 cells was time- and temperature-dependent (Fig. 5). The resident and elicited Mϕs showed a significantly higher cellular association of ^{32}P-labelled pDNA at both 4° and 37° than observed in the RAW264.7 and J774A1 cell lines. In the confocal microscopy study, fluorescein-labelled pDNA was also taken up by both RAW264.7 cells and resident Mϕs. The latter took up pDNA more efficiently (Fig. 5).

After endocytosis, DNA is degraded by deoxyribonuclease II (DNAse II) in the lysosomal compartment[31] and this event may affect the recognition of CpG motifs by TLR-9 in Mϕs. Therefore, the difference in degradation efficiency may account for the distinct responsiveness between primary Mϕs and cell lines. To explore the effect of degradation of pDNA on immunoactivation, we measured the amount of ^{32}P-labelled pDNA degraded by RAW264.7 cells and resident Mϕs by the TCA precipitation method. The TCA-soluble degradation products will be small DNA fragments (short oligodeoxynucleotides), as

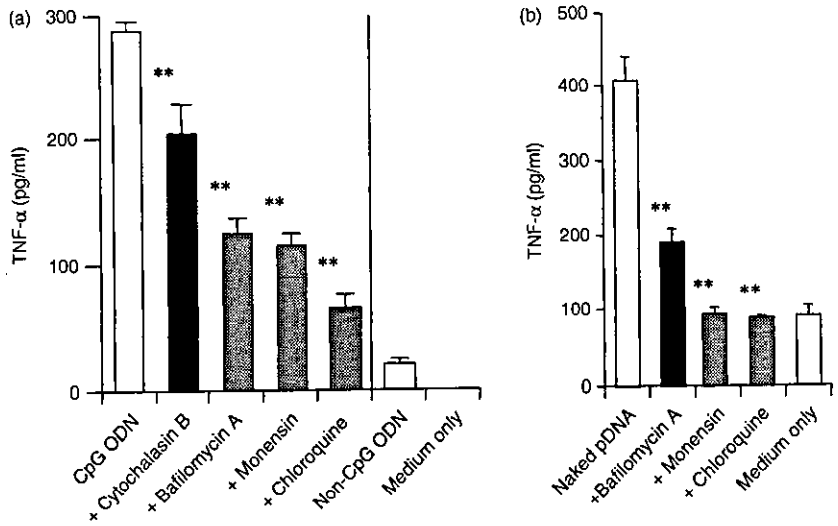

Figure 4. Tumour necrosis factor-α (TNF-α) release induced by CpG oligodeoxynucleotides (ODN) or non-CpG ODN from resident macrophages (Mϕs) (a) or plasmid DNA (pDNA) from RAW264.7 cells (b). (a) Resident Mϕs were incubated with 10 μM CpG ODN or non-CpG ODN, in the presence or absence of inhibitors, at 37° for 8 hr. (b) RAW264.7 cells were incubated with 10 μg/ml CpG pDNA, in the presence or absence of inhibitors, at 37° for 2 hr. Each result represents the mean and standard deviation (n = 3). Differences in the cytokine levels of the samples treated with CpG ODN only and CpG ODN + inhibitors (bafilomycin A, cytochalasin B, chloroquine and monensin) were analysed statistically by using the Student's t-test. $^{**}P < 0{\cdot}01$.

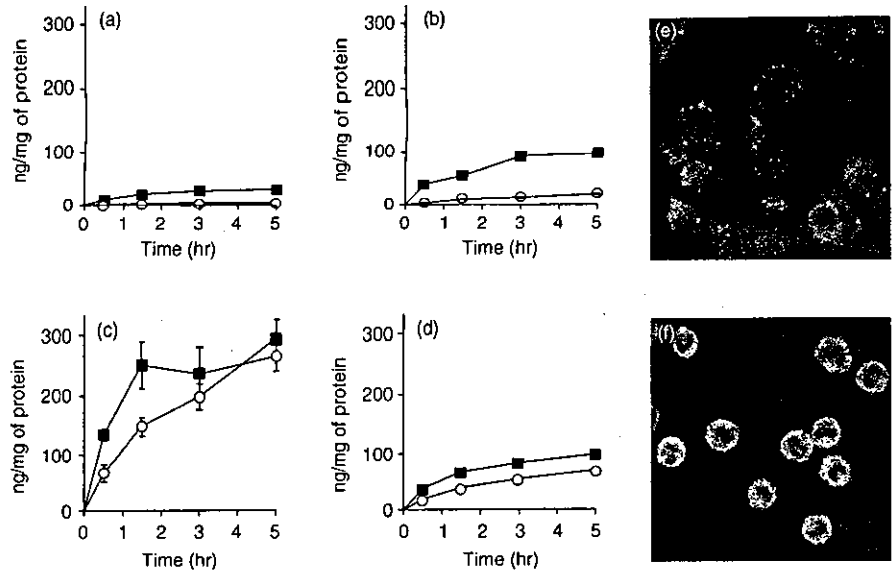

Figure 5. Cellular association time-course experiments of ^{32}P-labelled plasmid DNA (pDNA) in RAW264.7 cells (a), J774A1 cells (b), and resident (c) or elicited (d) macrophages (Mϕs); and cellular localization of pDNA in RAW264.7 cells (e) or resident Mϕs (f). (a–d) Cells were incubated with ^{32}P-labelled pDNA (0·1 μg/ml) at 37° (closed square) or 4° (open circle). Each point represents the mean ± standard deviation (n = 3). (e and f) Cells were incubated at 4° for 30 min in the presence of 5 μg/ml Texas Red-labelled pDNA. After washing, the cells were warmed to 37° to allow internalization for 15 min. Images represent laser-scanning confocal microscopy sections.

50% precipitation occurs with the 16-mer oligodeoxynucleotides.[32] Both RAW264.7 cells and resident Mϕs degraded the pDNA and released its degradation products into the medium to a similar extent (Fig. 6).

Single-stranded DNA or smaller DNA was unable to induce TNF-α production from peritoneal Mϕs

Resident peritoneal Mϕs were found to induce inflammatory cytokines by a small single-stranded CpG ODN (Fig. 4a), although they were unable to produce TNF-α following stimulation with larger double-stranded pDNA (Fig. 1). *E. coli* DNA is often used after sonication and heat denaturation.[3,5,7,33,34] We prepared small DNA fragments by sonication to examine whether the physicochemical properties of DNA affect the activation of Mϕs. pDNA fragments were reduced to less than 600 bp after sonication for 120 min (Fig. 7). In addition, pDNA, or its fragments, were denatured at 90° to prepare single-stranded DNA. In RAW264.7 cells, the amount of TNF-α released by DNA fragments was almost the same as

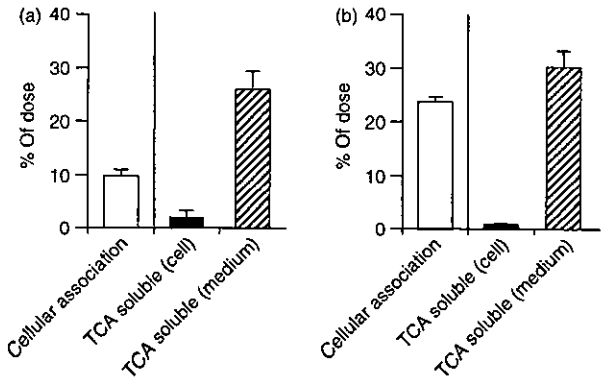

Figure 6. Degradation of ^{32}P-labelled plasmid DNA (pDNA) by RAW264.7 cells (a) or resident macrophages (Mϕs) (b). The cells were incubated with ^{32}P-labelled pDNA (0·1 μg/ml) at 37° or 4° for 3 hr. The degree of cellular association and degradation of ^{32}P-labelled pDNA was measured by the trichloroacetic acid (TCA) precipitation method. Each result represents the mean and standard deviation (n = 6).

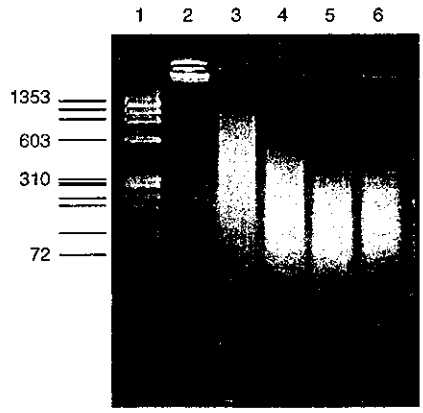

Figure 7. Electrophoresis of plasmid DNA (pDNA) fragments prepared by sonication. DNA mobility was analysed by agarose-gel electrophoresis (3·5% gel). Lane 1, Φ-*Hae*III marker; lane 2, control pCMV-Luc; lanes 3–6, pCMV-Luc fragments produced by sonication for 30, 60, 90 and 120 min, respectively.

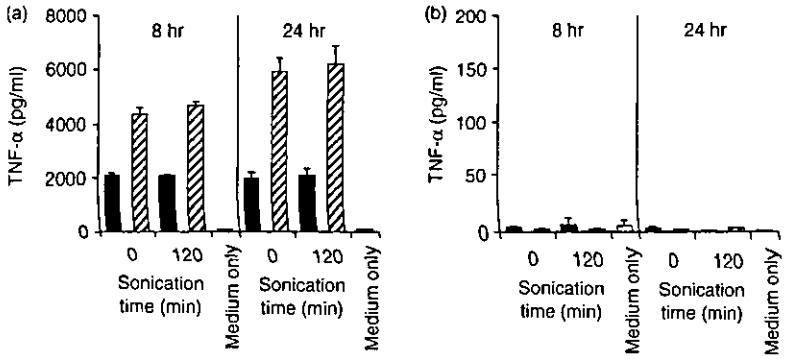

Figure 8. Cytokine release induced by plasmid DNA (pDNA) fragments or single-stranded DNA from RAW264.7 cells (a) or resident macrophages (Mϕs) (b). The cells were incubated with double-stranded DNA (black bar) or single-stranded DNA (hatched bar) for 8 hr. Cytokine release from Mϕs was quantified by enzyme-linked immunosorbent assay (ELISA). Each result represents the mean and standard deviation ($n = 6$).

that released by intact pDNA (Fig. 8). On the other hand, heat-denatured pDNA significantly increased TNF-α production from the Mϕ cell line, indicating that single-stranded DNA is a more potent cell activator. However, resident Mϕs could not secrete TNF-α upon stimulation with small-size pDNA or heat-denatured pDNA.

DISCUSSION

The important role of immunostimulatory effects mediated by the CpG motif in gene therapy and DNA vaccination has been well defined. However, most *in vitro* studies, focusing on the mechanisms of Mϕ activation mediated by CpG DNA, have been carried out using CpG ODN and bacterial genomic DNA in Mϕ cell lines.[28,35,36] Only a few reports have investigated immune responses induced by pDNA or bacterial DNA from Mϕs or monocytes in primary culture.[37–39]

In the present study, we used Triton X-114 to remove LPS from DNA samples. Naked pDNA and *E. coli* genomic DNA containing unmethylated CpG motifs were able to stimulate the Mϕ cell lines RAW264.7 and J774A1 to produce a significant amount of TNF-α (Fig. 2), while mammalian calf thymus DNA, which does not contain immunostimulatory CpG motifs, could not stimulate TNF-α production from these cell lines. Inhibitors of endocytosis and endosomal acidification prevented the pDNA-stimulated release of TNF-α from RAW264.7 cells (Fig. 4b). Therefore, it is probable that pDNA activates RAW264.7 cells to secrete cytokines by the same mechanism as that reported for CpG ODN.[28]

On the other hand, the resident and elicited Mϕs from male ICR mice did not show any TNF-α or IL-6 induction by naked pDNA or *E. coli* DNA, even when exposed to a very high concentration of these DNAs (Fig. 1). Similar results were observed in the resident Mϕs isolated from female ICR and male C3H/HeJ (LPS non-responders) and C3H/HeN mice (data not shown). Peritoneal Mϕs primed by interferon-γ (IFN-γ) also showed similar results, although increased TNF-α secretion induced by LPS was observed in the primed cells (data not shown). This unresponsiveness of primary Mϕs disagreed with previous reports.[5,38] Bone marrow-derived Mϕs can respond to pDNA,[38] and only 1 μg/ml pDNA can induce NF-κB activation and TNF-α production in such Mϕs. It may be that peritoneal Mϕs and bone marrow-derived Mϕs exhibit different responses to pDNA. Another report shows that DNA from Gram-positive *Staphylococcus aureus* can activate peritoneal Mϕs of C3H/HeJ mice to produce TNF-α.[5] *S. aureus* DNA may contain higher numbers or more potent CpG motifs than Gram-negative *E. coli* DNA or the pDNA that we used. Further studies are required to explain these contradictions. The very low, almost negligible, induction of cytokine upon stimulation with naked DNA was in complete contrast to our recent findings on DNA/cationic liposome complexes.[21] Both the resident peritoneal Mϕs and RAW264.7 cells secreted a large amount of TNF-α following incubation with pDNA and *E. coli* DNA complexed with LipofectAMINE plus. Also of note, similar cytokine induction was evoked in both resident peritoneal Mϕs and RAW264.7 cells by the complexes prepared with calf thymus DNA and methylated-CpG pDNA, indicating that the Mϕ activation was a CpG motif-independent process.

The restricted induction of cytokines by naked pDNA was not a result of the lack of TLR-9 expression in the peritoneal Mϕs (Fig. 3), which is responsible for recognition of the bacterial CpG DNA.[14,15] Indeed, the Mϕ can release TNF-α in a CpG motif-dependent manner (Fig. 4), as previously reported.[4,38] Therefore, the resident Mϕs have the ability to respond to CpG DNA.

CpG DNA should be taken up by Mϕs and, thereafter, be transported to the endosomal/lysosomal compartment for recognition by TLR-9.[30] pDNA was efficiently taken up and degraded into smaller DNA fragments by the resident peritoneal Mϕs (Figs 5 and 6). The pDNA degradation would be mediated by DNAse II in the lysosomal compartment of the Mϕs.[31,40,41] However, the apparent uptake efficiency of pDNA by the resident Mϕs appeared to be higher that that of RAW264.7 cells. Therefore, the very low responsiveness to pDNA was not a result of impaired cellular uptake of the CpG DNA by the peritoneal Mϕs.

In cellular activation experiments, *E. coli* DNA is often used after sonication and heat denaturation.[3,5,7,33,34] Heat-denatured (single-stranded) *E. coli* DNA was 10–30% more mitogenic than double-stranded DNA as far as B cells were concerned.[34] In fact, in the present study, RAW264.7 cells were stimulated to

produce about twice as much TNF-α by single-stranded pDNA compared with double-stranded pDNA (Fig. 8a). On the other hand, DNA fragments prepared by sonication resulted in a similar level of TNF-α secretion compared with control pDNA. This was in agreement with a previous report that mycobaterial DNA fragments generated by digestion with restriction enzyme or the fragments prepared by sonication do not modify IL-12 induction by THP-1 monocytes.[42] Heat-denatured single-stranded pDNA, which exhibited a greater ability to induce TNF-α in RAW264.7 cells, could not stimulate resident Mϕs to induce inflammatory cytokines (Fig. 8a).

The findings of the present study suggest that peritoneal Mϕs, or other Mϕs such as Kupffer cells, may play an insignificant role in cytokine production through direct activation by naked pDNA *in vivo*. pDNA is efficiently taken up by the liver when it is injected into mice, and hepatic accumulation has been found to occur preferentially in the non-parenchymal cells, including Kupffer cells (liver Mϕs).[18] When mice are sensitized with D-galactosamine they suffer from lethal toxic shock as a result of TNF-α, induced by bacterial DNA, producing fulminant apoptosis of liver cells.[5] However, a very large dose (300 μg/mouse) is required to produce this shock. Moreover, bacterial DNA alone is less toxic and cannot induce lethal shock without LPS or D-galactosamine treatment.[43] These observations are in agreement with our speculation involving restricted cytokine production by direct pDNA stimulation from Mϕs *in vivo*.

The restricted cytokine induction by naked pDNA also contrasts with our recent observation of DCs in culture. Significant production of inflammatory cytokines, such as TNF-α, IL-6 and IL-12, was induced by naked pDNA and *E. coli* DNA, but not by calf thymus DNA, from both bone marrow-derived DCs in primary culture and a DC cell line, DC2.4.[44] Neither type of DC displayed CpG motif-independent cytokine secretion upon stimulation with DNA/cationic liposome complexes. Therefore, DCs, another important cell population for DNA-based therapies, show CpG motif-dependent cyokine production against pDNA, regardless of whether the cells are in primary culture or of a cell line. Mϕs have features distinct from DCs in terms of cytokine induction by pDNA.

In conclusion, the present study demonstrated that primary cultured mouse peritoneal Mϕs and Mϕ cell lines exhibit significantly different responses to pDNA as far as inflammatory cytokine induction is concerned. In contrast to the cell lines, the peritoneal Mϕs secreted almost no inflammatory cytokines (TNF-α, IL-6) upon stimulation with pDNA, in spite of extensive uptake of the CpG DNA. These findings have important implications for Mϕ activation by naked pDNA in DNA-based therapies because it has been generally assumed that pDNA-containing CpG motifs are potent agents for inducing inflammatory cytokines *in vivo* based on information from *in vitro* studies using Mϕ cell lines.

ACKNOWLEDGMENTS

This work was supported in part by a grant-in-aid for Scientific Research from the Ministry of Education, Culture, Sports, Sciences and Technology, Japan.

REFERENCES

1 Krieg AM, Kline JN. Immune effects and therapeutic applications of CpG motifs in bacterial DNA. Immunopharmacology 2000; **48**:303.
2 Wagner H. Immunobiology of Bacterial CpG-DNA. In: Wagner H, ed. Current Topics in Microbiology and Immunology, Vol 247. Berlin: Springer, 1999.
3 Yi AK, Klinman DM, Martin TL, Matson S, Krieg AM. Rapid immune activation by CpG motifs in bacterial DNA. Systemic induction of IL-6 transcription through an antioxidant-sensitive pathway. J Immunol 1996; **157**:5394.
4 Sparwasser T, Miethke T, Lipford G, Borschert K, Hacker H, Heeg K, Wagner H. Bacterial DNA causes septic shock. Nature 1997; **386**:336.
5 Sparwasser T, Miethke T, Lipford G, Erdmann A, Hacker H, Heeg K, Wagner H. Macrophages sense pathogens via DNA motifs: induction of tumor necrosis factor-alpha-mediated shock. Eur J Immunol 1997; **27**:1671.
6 Krieg AM, Love HL, Yi AK, Harty JT. CpG DNA induces sustained IL-12 expression *in vivo* and resistance to *Listeria monocytogenes* challenge. J Immunol 1998; **161**:2428.
7 Klinman DM, Yi AK, Beaucage SL, Conover J, Krieg AM. CpG motifs present in bacteria DNA rapidly induce lymphocytes to secrete interleukin 6, interleukin 12, and interferon gamma. Proc Natl Acad Sci USA 1996; **93**:2879.
8 Singh M, O'Hagan D. Advances in vaccine adjuvants. Nat Biotechnol 1999; **17**:1075.
9 Weeratna RD, McCluskie MJ, Xu Y, Davis HL. CpG DNA induces stronger immune responses with less toxicity than other adjuvants. Vaccine 2000; **18**:1755.
10 Raz E, Tighe H, Sato Y *et al.* Preferential induction of a Th1 immune response and inhibition of specific IgE antibody formation by plasmid DNA immunization. Proc Natl Acad Sci USA 1996; **93**:5141.
11 Roman M, Martin OE, Goodman JS *et al.* Immunostimulatory DNA sequences function as T helper-1-promoting adjuvants. Nat Med 1997; **3**:849.
12 Qin L, Ding Y, Pahud DR, Chang E, Imperiale MJ, Bromberg JS. Promoter attenuation in gene therapy: interferon-gamma and tumor necrosis factor-alpha inhibit transgene expression. Hum Gene Ther 1997; **8**:2019.
13 Ghazizadeh S, Carroll JM, Taichman LB. Repression of retrovirus-mediated transgene expression by interferons: implications for gene therapy. J Virol 1997; **71**:9163.
14 Hemmi H, Takeuchi O, Kawai T *et al.* A Toll-like receptor recognizes bacterial DNA. Nature 2000; **408**:740.
15 Bauer S, Kirschning CJ, Hacker H, Redecke V, Hausmann S, Akira S, Wagner H, Lipford GB. Human TLR9 confers responsiveness to bacterial DNA via species-specific CpG motif recognition. Proc Natl Acad Sci USA 2001; **98**:9237.
16 Hacker H, Vabulas RM, Takeuchi O, Hoshino K, Akira S, Wagner H. Immune cell activation by bacterial CpG-DNA through myeloid differentiation marker 88 and tumor necrosis factor receptor-associated factor (TRAF) 6. J Exp Med 2000; **192**:595.
17 Baud V, Liu ZG, Bennett B, Suzuki N, Xia Y, Karin M. Signaling by proinflammatory cytokines: oligomerization of TRAF2 and TRAF6 is sufficient for JNK and IKK activation and target gene induction via an amino-terminal effector domain. Genes Dev 1999; **13**:1297.
18 Kawabata K, Takakura Y, Hashida M. The fate of plasmid DNA after intravenous injection in mice: involvement of scavenger receptors in its hepatic uptake. Pharm Res 1995; **12**:825.
19 Takagi T, Hashiguchi M, Mahato RI, Tokuda H, Takakura Y, Hashida M. Involvement of specific mechanism in plasmid DNA

uptake by mouse peritoneal macrophages. Biochem Biophys Res Commun 1998; **245**:729.

20 Takakura Y, Takagi T, Hashiguchi M *et al.* Characterization of plasmid DNA binding and uptake by peritoneal macrophages from class A scavenger receptor knockout mice. Pharm Res 1999; **16**:503.

21 Yasuda K, Ogawa Y, Kishimoto M, Takagi T, Hashida M, Takakura Y. Plasmid DNA activates murine macrophages to induce inflammatory cytokines in a CpG motif-independent manner by complex formation with cationic liposomes. Biochem Biophys Res Commun 2002; **293**:344.

22 Nomura T, Yasuda K, Yamada T, Okamoto S, Mahato RI, Watanabe Y, Takakura Y, Hashida M. Gene expression and antitumor effects following direct interferon (IFN)-gamma gene transfer with naked plasmid DNA and DC-chol liposome complexes in mice. Gene Ther 1999; **6**:121.

23 Rigby PW, Dieckmann M, Rhodes C, Berg P. Labeling deoxyribonucleic acid to high specific activity *in vitro* by nick translation with DNA polymerase I. J Mol Biol 1977; **113**:237.

24 Cotten M, Baker A, Saltik M, Wagner E, Buschle M. Lipopolysaccharide is a frequent contaminant of plasmid DNA preparations and can be toxic to primary human cells in the presence of adenovirus. Gene Ther 1994; **1**:239.

25 Hartmann G, Krieg AM. CpG DNA and LPS induce distinct patterns of activation in human monocytes. Gene Ther 1999; **6**:893.

26 Krieg AM, Yi AK, Matson S, Waldschmidt TJ, Bishop GA, Teasdale R, Koretzky GA, Klinman DM. CpG motifs in bacterial DNA trigger direct B-cell activation. Nature 1995; **374**:546.

27 Wang C, Smith RL. Lowry determination of protein in the presence of Triton X-100. Anal Biochem 1975; **63**:414.

28 Yi AK, Tuetken R, Redford T, Waldschmidt M, Kirsch J, Krieg AM. CpG motifs in bacterial DNA activate leukocytes through the pH-dependent generation of reactive oxygen species. J Immunol 1998; **160**:4755.

29 Hacker H, Mischak H, Miethke T *et al.* CpG-DNA-specific activation of antigen-presenting cells requires stress kinase activity and is preceded by non-specific endocytosis and endosomal maturation. EMBO J 1998; **17**:6230.

30 Ahmad-Nejad P, Hacker H, Rutz M, Bauer S, Vabulas RM, Wagner H. Bacterial CpG-DNA and lipopolysaccharides activate Toll-like receptors at distinct cellular compartments. Eur J Immunol 2002; **32**:1958.

31 Krieser RJ, Eastman A. The cloning and expression of human deoxyribonuclease II. A possible role in apoptosis. J Biol Chem 1998; **273**:30909.

32 Cleaver JE, Boyer HW. Solubility and dialysis limits of DNA oligonucleotides. Biochim Biophys Acta 1972; **262**:116.

33 Schwartz DA, Quinn TJ, Thorne PS, Sayeed S, Yi AK, Krieg AM. CpG motifs in bacterial DNA cause inflammation in the lower respiratory tract. J Clin Invest 1997; **100**:68.

34 Sun S, Beard C, Jaenisch R, Jones P, Sprent J. Mitogenicity of DNA from different organisms for murine B cells. J Immunol 1997; **159**:3119.

35 Sester DP, Stacey KJ, Sweet MJ, Beasley SJ, Cronau SL, Hume DA. The actions of bacterial DNA on murine macrophages. J Leukoc Biol 1999; **66**:542.

36 Gao JJ, Zuvanich EG, Xue Q, Horn DL, Silverstein R, Morrison DC. Cutting edge: bacterial DNA and LPS act in synergy in inducing nitric oxide production in RAW264.7 macrophages. J Immunol 1999; **163**:4095.

37 Sweet MJ, Stacey KJ, Kakuda DK, Markovich D, Hume DA. IFN-gamma primes macrophage responses to bacterial DNA. J Interferon Cytokine Res 1998; **18**:263.

38 Stacey KJ, Sweet MJ, Hume DA. Macrophages ingest and are activated by bacterial DNA. J Immunol 1996; **157**:2116.

39 Bauer M, Heeg K, Wagner H, Lipford GB. DNA activates human immune cells through a CpG sequence-dependent manner. Immunology 1999; **97**:699.

40 Odaka C, Mizuochi T. Role of macrophage lysosomal enzymes in the degradation of nucleosomes of apoptotic cells. J Immunol 1999; **163**:5346.

41 McIlroy D, Tanaka M, Sakahira H *et al.* An auxiliary mode of apoptotic DNA fragmentation provided by phagocytes. Genes Dev 2000; **14**:549.

42 Filion MC, Filion B, Reader S, Menard S, Phillips NC. Modulation of interleukin-12 synthesis by DNA lacking the CpG motif and present in a mycobacterial cell wall complex. Cancer Immunol Immunother 2000; **49**:325.

43 Cowdery JS, Chace JH, Yi AK, Krieg AM. Bacterial DNA induces NK cells to produce IFN-gamma *in vivo* and increases the toxicity of lipopolysaccharides. J Immunol 1996; **156**:4570.

44 Yoshinaga T, Yasuda K, Ogawa Y, Takakura Y. Efficient uptake and rapid degradation of plasmid DNA by murine dendritic cells via a specific mechanism. Biochem Biophys Res Commun 2002; **299**:389.

Inhibition of Metastatic Tumor Growth in Mouse Lung by Repeated Administration of Polyethylene Glycol-Conjugated Catalase: Quantitative Analysis with Firefly Luciferase-Expressing Melanoma Cells

Kenji Hyoudou,[1] Makiya Nishikawa,[2] Yukari Umeyama,[1] Yuki Kobayashi,[1] Fumiyoshi Yamashita,[1] and Mitsuru Hashida[1]

Department of [1]Drug Delivery Research, and [2]Biopharmaceutics and Drug Metabolism, Graduate School of Pharmaceutical Sciences, Kyoto University, Kyoto, Japan

ABSTRACT

Purpose: **To develop a novel and effective approach to inhibit tumor metastasis based on controlled delivery of catalase, we first evaluated the characteristics of the disposition and proliferation of tumor cells. Then, we examined the effects of polyethylene glycol-conjugated catalase (PEG-catalase) on tumor metastasis. On the basis of the results obtained, PEG-catalase was repetitively administered to completely suppress the growth of tumor cells.**

Experimental Design: **Murine melanoma B16-BL6 cells were stably transfected with *firefly luciferase* gene to obtain B16-BL6/Luc cells. These cells were injected intravenously into syngeneic C57BL/6 mice. PEG-catalase was injected intravenously, and the effect was evaluated by measuring the luciferase activity as the indicator of the number of tumor cells.**

Results: **At 1 hour after injection of B16-BL6/Luc cells, 60 to 90% of the injected cells were recovered in the lung. The numbers decreased to 2 to 4% at 24 hours, then increased. An injection of PEG-catalase just before inoculation significantly reduced the number of tumor cells at 24 hours. Injection of PEG-catalase at 1 or 3 days after inoculation was also effective in reducing the cell numbers. Daily dosing of PEG-catalase greatly inhibited the proliferation and the number assayed at 14 days after inoculation was not significantly different from the minimal number observed at 1 day, suggesting that the growth had been markedly suppressed by the treatment.**

Conclusions: **These findings indicate that sustained catalase activity in the blood circulation can prevent the multiple processes of tumor metastasis in the lung, which could lead to a state of tumor dormancy.**

INTRODUCTION

Tumor metastasis is the major cause of death in cancer patients. It can be roughly divided into the following steps: tumor cell dissociation, invasion, intravasation, distribution to distant organs, arrest in small vessels, adhesion to endothelial cells, extravasation, invasion of the target organ and proliferation (1). Adhesion of circulating tumor cells to capillary endothelial cells is a crucial event in the retention of tumor cells in a specific organ (2). Initial interactions between tumor cells and endothelium activates both tumor cells and endothelial cells through cytokines, free radicals, bioactive lipids, and growth factors, leading to the increased expression of adhesion molecules, which strengthens the initial adhesive bonds (3, 4). Reactive oxygen species (ROS), such as hydrogen peroxide (H_2O_2), superoxide anion and hydroxyl radical, are well known regulators of such adhesion molecules (5–7).

In most cases, the lung is the first organ that tumor cells detached from primary tumors encounter, making it a major site for tumor metastasis. We have shown that an experimental pulmonary metastasis of colon carcinoma cells in mice can be effectively inhibited by polyethylene glycol-conjugated catalase (PEG-catalase; ref. 8). The number of metastatic colonies on the lung surface was significantly lower in mice treated with PEG-catalase than in untreated (saline-injected) mice. However, the mechanism of this inhibition is not clear because ROS are involved in various metastatic processes, such as adhesion (5, 6), invasion (9–11), and proliferation (12). Counting visible metastatic colonies on the tissue surface is not sensitive enough to evaluate these early processes of tumor metastasis. In an attempt to circumvent this problem, radiolabeled tumor cells are sometimes used to trace their disposition *in vivo*, but cell death as well as the release of radiolabeled compounds from cells make it very difficult to analyze the disposition of tumor cells. Furthermore, tumor growth cannot be evaluated by this approach.

Labeling of cells with any protein by introducing its gene has been applied to studies of tumor metastasis. This technique is very promising in evaluating tumor metastasis because the protein introduced can be tumor cell-specific. Thus far, several authors have already used this kind of experimental system to

Received 5/25/04; revised 7/24/04; accepted 7/29/04.
Grant support: Grants-in-Aid for Scientific Research from the Ministry of Education, Culture, Sports, Science, and Technology of Japan (No. 15025233), by Health and Labor Sciences Research Grants for Research on Hepatitis and Bovine Spongiform Encephalopathy from the Ministry of Health, Labor, and Welfare of Japan (No. 15–21) and by the 21st Century Center of Excellence Program "Knowledge Information Infrastructure for Genome Science."
The costs of publication of this article were defrayed in part by the payment of page charges. This article must therefore be hereby marked *advertisement* in accordance with 18 U.S.C. Section 1734 solely to indicate this fact.
Requests for reprints: Mitsuru Hashida, Department of Drug Delivery Research, Graduate School of Pharmaceutical Sciences, Kyoto University, Sakyo-ku, Kyoto, Japan. Phone: 81-75-753-4545; Fax: 81-75-753-4575; E-mail: hashidam@pharm.kyoto-u.ac.jp.

show the growth of tumor cells *in vivo* (13, 14) and metastasis by *in vivo* imaging (14–17). However, there have been few investigations of the early processes of tumor metastasis, such as the embolization, adhesion, and invasion, using these reporter gene-labeled tumor cells. These processes cannot be evaluated by *in vivo* imaging because of a lack of sensitivity and its less quantitative nature. Reporter gene assays can solve these problems if tumor cells are stably transfected at a high level of specific activity. In addition, the reporter gene expression should be constant under a variety of conditions to use the activity as a scale for the number of tumor cells *in vivo*.

In the present study, we first developed clones of murine melanoma B16-BL6 cells by transfecting firefly luciferase gene. The characteristics of the transfectant, B16-BL6/Luc cells, were examined *in vitro* as well as *in vivo*, and we found that the transfectant can be used to examine the disposition and proliferation of tumor cells *in vivo*. Therefore, the processes of tumor metastasis were examined in mice by measuring the luciferase activity in the lung after intravenous administration of the cells. Finally, the effects of catalase and PEG-catalase on early as well as later processes of tumor metastasis were evaluated in this system. To our knowledge, this is the first report showing that repeated injection of PEG-catalase almost completely suppresses the growth of metastatic tumors in the lung. These findings suggest that tumor dormancy may be induced by continuous administration of PEG-catalase.

MATERIALS AND METHODS

Animals. Male C57/BL6 (6-week-old) mice were purchased from the Shizuoka Agricultural Cooperative Association for Laboratory Animals (Shizuoka, Japan). Animals were maintained under conventional housing conditions. All animal experiments were conducted in accordance with the principles and procedures outlined in the United States NIH Guide for the Care and Use of Laboratory Animals. The protocols for animal experiments were approved by the Animal Experimentation Committee of Graduate School of Pharmaceutical Sciences of Kyoto University.

Chemicals. DMEM and HBSS were obtained from Nissui Pharmaceutical (Tokyo, Japan). Fetal bovine serum was obtained from Biowhittaker (Walkersville, MD). Bovine liver catalase (C-100, 40,000 units/mg) was purchased from Sigma Chemical (St. Louis, MO). A product of PEG [2,4-bis (*o*-methoxypolyethylene glycol)-6-chloro-s-triazin] was obtained from Seikagaku Corporation (Japan), and PEG-catalase and inactivated catalase were synthesized and their enzymatic activity measured as reported previously (18). All other chemicals were of the highest grade commercially available.

Tumor Cells. Murine melanoma B16-BL6 tumor cells (19), obtained from the Cancer Chemotherapy Center of the Japanese Foundation for Cancer Research (Tokyo, Japan), were grown in DMEM supplemented with 10% heat-inactivated fetal bovine serum, 0.15% $NaHCO_3$, 100 units/mL penicillin, and 100 μg/mL streptomycin at 37°C in humidified air containing 5% CO_2. To establish cell lines stably expressing firefly luciferase, B16-BL6 cells were transfected with plasmid DNA encoding *firefly luciferase* under the control of cytomegalovirus immediate early promoter (20) complexed with Lipofectamine2000 (Life Technologies, Inc.–Invitrogen). Then the cells were treated with medium containing 1 mg/mL G418 (Geneticin, Sigma) and single colonies of G418-resistant cells were picked up and examined for their luciferase activity as described below. On the basis of the luciferase activity, a clone was selected and its growth rate *in vitro* was compared with that of B16-BL6 cells. In addition, 1×10^5 cells of B16-BL6 or B16-BL6/Luc were injected into the lateral tail vein of mice. At 2 weeks after injection, the number of metastatic colonies on the lung surface was counted.

Disposition and Proliferation of B16-BL6/Luc Cells after Intravenous Injection in Mice. Into the lateral tail vein of mice were injected 1×10^3, 1×10^4, 1×10^5, 5×10^5 or 1×10^6 B16-BL6/Luc cells in 0.1 mL HBSS. At 1, 24 hours, 3, 7, and 14 days after tumor injection, mice were killed and the lung was excised, weighed, and the luciferase activity in the tissue was measured.

Effect of Catalase Derivatives on the Number of B16-BL6/Luc Cells in Mice. Experimental pulmonary metastasis was induced by injecting 1 or 5×10^5 B16-BL6/Luc cells in 0.1 mL of HBSS into the lateral tail vein of C57/BL6 mice. Saline (untreated, control group), catalase, PEG-catalase, or inactivated catalase was injected in the lateral tail vein at a dose of 1,000 catalase units unless otherwise indicated. At 24 hours after tumor injection, mice were killed, and the lung was excised, weighed, and the luciferase activity in the tissue was measured.

Separately, the effects of catalase on tumor metastasis at later periods were examined by measuring the luciferase activity of the lung at 7 days after tumor injection. Experimental pulmonary metastasis was induced by injecting 1×10^5 B16-BL6/Luc cells as described above. Then, saline or PEG-catalase was injected just before, and 1 or 3 days after tumor injection.

Multiple Dosing of PEG-Catalase. Experimental pulmonary metastasis was induced by injecting 1×10^4 B16-BL6/Luc cells in 0.1 mL of HBSS into the lateral tail vein of C57/BL6 mice. Saline (untreated, control group) or PEG-catalase was injected daily into the lateral tail vein at a dose of 1,000 catalase units/injection. At 2 weeks after tumor injection, mice were killed, and the lungs were excised, weighed, and the luciferase activity in the tissues was measured.

Separately, the effects of PEG-catalase on the survival of mice with lung metastases were examined. Experimental pulmonary metastasis was induced by injecting 1×10^4 B16-BL6/Luc cells as described above. Then, saline, PEG-catalase (1,000 catalase units), or bovine serum albumin (BSA; amount of protein equivalent to PEG-catalase) was injected daily into the lateral tail vein until 30 days after tumor injection.

Measurement of Luciferase Activity. The cells or tissues were homogenized with a lysis buffer [0.05% Triton X-100, 2 mmol/L EDTA, 0.1 mol/L Tris (pH 7.8)], and subjected to three cycles of freezing (liquid N_2 for 3 minutes) and thawing (37°C, 3 minutes), followed by centrifugation at $10,000 \times g$ for 10 minutes. Ten microliters of the supernatant was mixed with 100 μL of luciferase assay buffer (Picagene, Toyo Ink, Tokyo, Japan), and the light produced was immediately measured with a luminometer (Lumat LB 9507, EG & G Berthold, Bad Wildbad, Germany).

Statistical Analysis. Differences were statistically evaluated by one-way ANOVA followed by the Student-Newmann-

Keuls multiple comparison test and Kaplan-Meier analysis with a log-rank test to determine survival, and the level of statistical significance was $P < 0.05$.

RESULTS

Characteristics of B16-BL6/Luc Cells. A number of B16-BL6/Luc colonies were obtained with different levels of luciferase activity. A colony expressing high luciferase activity was selected, and the characteristics of the cells were examined. There was no significant difference in the growth rates of B16-BL6 and B16-BL6/Luc cells *in vitro* (data not shown). In addition, they were microscopically identical. When injected into the tail vein of mice, both types of cell induced comparable numbers of metastatic colonies at 14 days (5 ± 1 for B16-BL6 cells and 6 ± 2 for B16-BL6/Luc cells, $P > 0.05$). These results indicate that the characteristics of B16-BL6 cells are hardly altered during the procedure for preparing B16-BL6/Luc cells.

The luciferase activity was proportional to the number of cells [relative light units (RLU)/cell] over a wide range from 100 RLU to 10,000,000 RLU. Treatment of the cultured B16-BL6/Luc cells with H_2O_2 (10 μmol/L) or catalase (10,000 units/mL) for up to 7 hours hardly altered the luciferase activity of the cells (data not shown). The expression level of luciferase in the clone was stable for up to 1 year.

Disposition and Proliferation of B16-BL6/Luc Cells in Mouse Lung. The lung excised from untreated mice showed no significant luciferase activity (<100 RLU/10 μL of sample). The addition of B16-BL6/Luc cells to lung tissues proportionally increased the luciferase activity according to the number of the cells (data not shown), indicating that the luciferase activity of the tissue can be used as an indicator of the number of cells. On the basis of these findings, the luciferase activity measured was converted to the number of B16-BL6/Luc cells in the lung. The regression line gave a constant of 50 RLU/cell for the quantification of the number of tumor cells. Measuring the luciferase activity of lung homogenates mixed with B16-BL6/Luc cells showed that ≥60 cells were enough for the detection of B16-BL6/Luc cells (Fig. 1).

Figure 2 shows the number of B16-BL6/Luc cells in the lungs of mice after intravenous injection of different numbers of cells. At 1 hours, about 60 to 90% of the luciferase activity derived from the injected cells was recovered in the lung. Little luciferase activity was detected in other organs such as the liver and spleen (data not shown). At 24 hours, however, only 2 to 4% of the injected cells were detected in the lung. Thereafter, when ≥1×10^5 cells were injected, the number of tumor cells in the lung increased with time. However, the growth of the tumor cells was rather slow when small numbers of cells were injected. When mice were injected with 1×10^3 cells, the number of cells in the lung hardly changed with time up to 14 days.

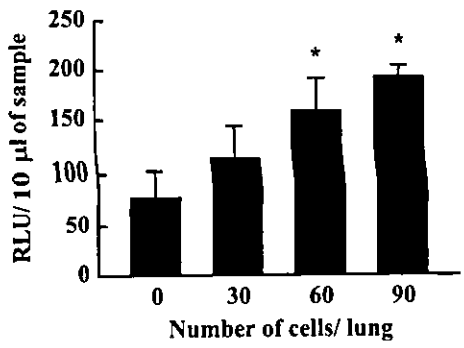

Fig. 1 Luciferase activity in the supernatant of homogenates of mouse lung mixed with different numbers of B16-BL6/Luc cells. Results are expressed as the mean ± SD of three samples. *, a statistically significant difference compared with the mouse lung without tumor cells ($P < 0.001$).

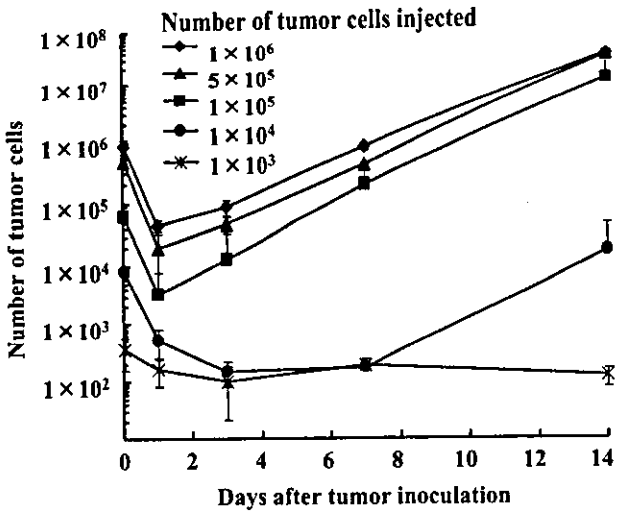

Fig. 2 Number of tumor cells in mouse lung after inoculation of B16-BL6/Luc cells into the tail vein at numbers of 1×10^6, 5×10^5, 1×10^5, 1×10^4, or 1×10^3 B16-BL6/Luc cells. Results are expressed as the mean ± SD of at least 3 mice.

Effect of Catalase Derivatives on the Number of B16-BL6/Luc Cells in Mouse Lung at 24 hours. It was found that the number of tumor cells was minimal at 24 hours after injection of B16-BL6/Luc cells. Then, we investigated whether catalase derivatives were able to reduce the number of tumor cells as early as 24 hour after the intravenous injection of 1×10^5 B16-BL6/Luc cells (Fig. 3*A*). An intravenous injection of catalase at a dose of 1,000 units/mouse tended to reduce the number of the tumor cells in the lung from 1.5×10^4 cells to 1.1×10^4 cells, but the difference was not significant. However, PEG-catalase had a greater inhibitory effect on the number of the tumor cells in the lung than catalase; only 0.50×10^4 cells were detected at 24 hours after tumor injection ($P < 0.05$ compared with the saline-treatment or catalase-treatment group).

In a separate set of experiments, PEG-catalase was injected at doses ranging from 100 to 10,000 units/mouse. The lowest dose of PEG-catalase was also effective in reducing the number of tumor cells in the lung (Fig. 3*B*). The number of the cells in the lung was proportional to the dose of PEG-catalase, suggesting that the detoxification of H_2O_2 inhibits the tumor cell survival in the lung. Inactivated catalase injected at a dose equivalent to 10,000 units catalase had no effect on metastasis.

Effect of Catalase on the Number of B16-BL6/Luc Cells in Mouse Lung at 7 Days. As shown in Fig. 2, the tumor cells in the lung were in a logarithmic growth phase at 24 h or later.

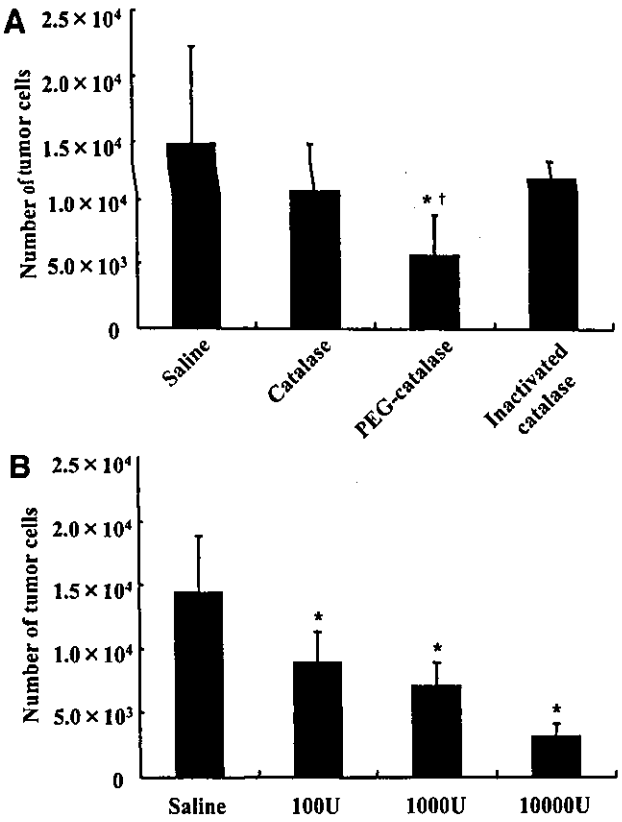

Fig. 3 Effect of catalase derivatives on the number of B16-BL6/Luc cells in mouse lung at 24 hours after inoculation of B16-BL6/Luc cells (5×10^5 cells) into the tail vein. Mice were killed at 24 hours after tumor injection and the luciferase activity in the lung was assayed. Results are expressed as the mean + SD of at least 6 mice. *A*, saline (vehicle), catalase, PEG-catalase (1,000 units/mouse) or inactivated catalase was injected into the tail vein of mice just beforethe injection of B16-BL6/Luc cells. *, a statistically significant difference compared with the saline group ($P < 0.05$); †, a statistically significant difference compared with the catalase group ($P < 0.05$). *B*, saline (vehicle) or PEG-catalase (100, 1,000, 10,000 units/mouse) was intravenously injected into mice just beforethe injection of B16-BL6/Luc cells. *, a statistically significant difference compared with the saline group ($P < 0.01$).

Therefore, at any time point around 24 h after injection, the tumor cells that survived appeared to adhere already to the endothelial cells and be ready for invasion and proliferation. To examine the effect of catalase on these tumor metastatic processes, PEG-catalase was injected at 1 or 3 days after tumor injection and the number of the tumor cells was measured at 7 days (Fig. 4). An intravenous injection of PEG-catalase at a dose of 1,000 units/mouse significantly reduced the number of tumor cells in the lung in both cases ($P < 0.005$ compared with the saline-treatment group). In addition, triple injections of PEG-catalase (total 3,000 units/mouse) further reduced the number of tumor cells ($P < 0.05$ compared with any other group), suggesting that the inhibitory effects of PEG-catalase at different periods are additive.

Inhibition of Tumor Cell Growth in Mouse Lung by Daily Injection of PEG-Catalase. It was found that PEG-catalase inhibits not only the early processes of metastasis, such as the adhesion of tumor cells, but also later processes like invasion and proliferation. Then, we investigated whether multiple injections of PEG-catalase were able to inhibit the growth of metastatic tumor cells in the lung. To the mice given an intravenous injection of 1×10^4 B16-BL6/Luc cells, PEG-catalase was injected at a dose of 1,000 units/injection each day from day 0 to day 14. This treatment resulted in a few tumor cells in the lung at 14 days after tumor inoculation (Fig. 5*A*). Furthermore, compared with the results of Fig. 2, the number of the cells in the lung of PEG-catalase–treated mice was not significantly different from that observed at 24 hours after tumor injection ($P > 0.05$). In addition, no metastatic colonies were seen under a dissecting microscope (Fig. 5*B*). Therefore, this suggests that the growth of tumor cells in the lung is almost completely inhibited by a daily injection of PEG-catalase.

Figure 6 shows the survival of mice receiving an intravenous injection of 1×10^4 B16-BL6 (parent) cells. Daily injection of PEG-catalase up to 30 days after tumor inoculation significantly prolonged the survival time of mice with B16-BL6 lung metastases compared with the saline- or BSA-treatment group ($P < 0.0001$ for the saline-treatment group, $P < 0.01$ for the BSA-treatment group).

DISCUSSION

Although metastasis is a major target of cancer therapy, it is difficult to treat metastases effectively. One of the major reasons for this is that the tissue disposition of tumor cells *in vivo* is poorly understood even in animal models. Metastasis consists of a number of different processes, such as adhesion, invasion, proliferation, and angiogenesis. Therefore, any inhib-

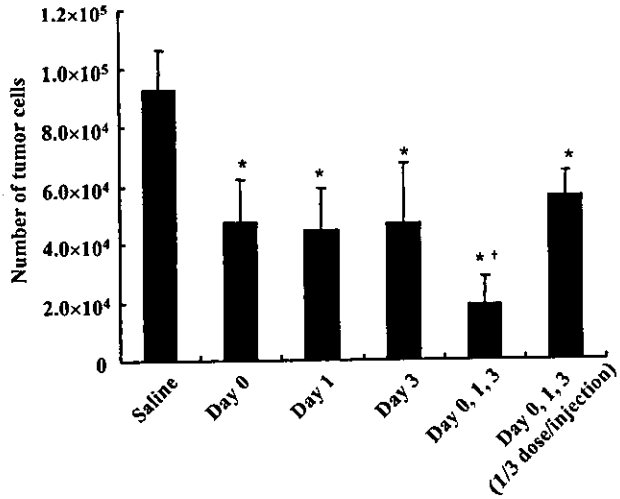

Fig. 4 Effect of injection timing of PEG-catalase on pulmonary metastasis of B16-BL6/Luc cells in mice. Saline (vehicle) or PEG-catalase (1,000 or 333 units/injection) was intravenously injected into mice just before (day 0), or 1 or 3 days after injection of B16-BL6/Luc cells (1×10^5 cells) into the tail vein. Mice were killed at 7 days after tumor injection and the luciferase activity in the lung was assayed. Results are expressed as the mean + SD of at least 6 mice. *, a statistically significant difference compared with the saline group ($P < 0.005$); †, a statistically significant difference compared with any other group ($P < 0.05$).

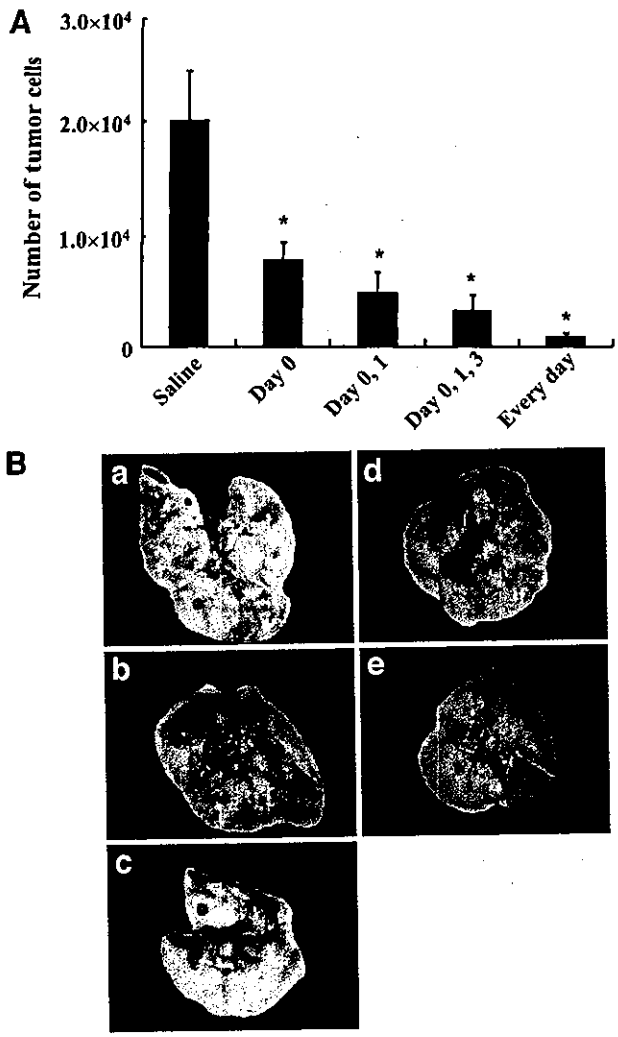

Fig. 5 Effect of multiple dosing of PEG-catalase on pulmonary metastasis in mice. *A*, saline (vehicle) or PEG-catalase (1,000 units/injection) was intravenously injected into mice in the schedule indicated after injection of B16-BL6/Luc cells (1×10^4 cells) into the tail vein. Mice were killed at 14 days after tumor injection and the luciferase activity in the lung was assayed. Results are expressed as the mean + SD of at least 6 mice. *, a statistically significant difference compared with the saline group ($P < 0.001$). *B*, Typical examples of pulmonary metastases in mice receiving an intravenous injection of 1×10^4 B16-BL6/Luc tumor cells followed by an injection of PEG-catalase. (*a*) Saline (vehicle), (*b*) PEG-catalase (day 0), (*c*) PEG-catalase (day 0, 1), (*d*) PEG-catalase (day 0, 1, 3), (*e*) PEG-catalase (every day). Each catalase derivative was injected into the tail vein at a dose of 1,000 units/injection.

itor of one of these processes could be an antimetastatic compound. Because the metastatic event results from interactions between tumor cells and other cells, methods analyzing the tissue disposition of tumor cells need to be developed to establish effective approaches for treating tumor metastasis. To this end, we introduced *firefly luciferase* gene into B16-BL6 cells as a marker, and established a highly sensitive and quantitative method to analyze the tissue disposition of tumor cells. Although the use of reporter gene-labeled tumor cells is not a novel approach to studying tumor growth and metastasis, until now there has been little published information on the separate processes of tumor metastasis. Therefore, in this study, we first examined the tissue disposition of B16-BL6/Luc cells after intravenous injection and identified the characteristic features of the *in vivo* fate of the cells. Then, we applied this analytical system to elucidate the mechanism whereby PEG-catalase reduces the number of metastatic colonies in the lung.

There are several requirements for the transfectant to use the luciferase activity in tissues as an indicator of the number of tumor cells. First, the expression level of luciferase should be high enough to ensure that a few cells can be detected *in vivo*. Second, the expression must be stable for a long period even after inoculation in mice. Furthermore, the expression should be independent of stimuli such as cytokines or ROS and of cell cycles. Finally, it is best that the characteristics of the transfectant do not differ from those of the parent cell line. Before *in vivo* studies, we examined the characteristics of the transfectant, B16-BL6/Luc cells. The luciferase activity of the cells was stable for at least 1 year and proportional to the cell number over a wide range. The expression of the luciferase in the cells was hardly affected by the growth phase, the addition of H_2O_2, or catalase. These properties are consistent with previous results showing that for plasmid DNA encoding *firefly luciferase* under the control of cytomegalovirus, immediate early promoter activity was independent of the cell cycle (21), and the expression level was scarcely affected after inoculation into mice (22). In addition, the half-life of firefly luciferase is very short (about 3 hours); therefore, the level of the luciferase protein in the cell would level off quickly. These properties enable us to use the luciferase activity in lung tissue as an indicator of the exact number of tumor cells.

In the experimental pulmonary metastasis model, B16-BL6 or B16-BL6/Luc melanoma cells were injected intravenously into syngeneic C57BL/6 mice. Therefore, the first step in the pulmonary metastasis is the arrest of the tumor cells in small vessels in the lung followed by their adhesion to endothelial cells (1, 23). As shown in Fig. 2, intravenous injection of B16-BL6/Luc cells resulted in the accumulation of 60 to 90% of the injected cells in the lung and few in other organs at 1 hour after tumor injection. Thereafter, the tumor cells in the lung fell to 2 to 4% of the injected cells at 24 hours. In contrast, when injected into the portal vein, about 60% of the injected B16-BL6/Luc cells were detected even at 24 hours after injection.[3] These results of organ- or cell number-independent tumor cell arrest suggest that the initial step in the formation of metastatic colonies of B16 tumor cells is mediated by physical trapping of the cells within the microvasculature of organs rather than by a specific interaction between tumor cells and endothelial cells via adhesion molecules. The tumor cells arrested in the lung could be destroyed in the microvasculature by mechanical stress caused by respiration in the first 24 hours after tumor injection. Because the injected tumor cells decreased to 2–4% irrespective of the initial number of cells, this inefficiency could be because of the physical forces of contraction and relaxation of the lung tissue but not to immunity. It is also suggested that at 24 hours

[3] Unpublished data.

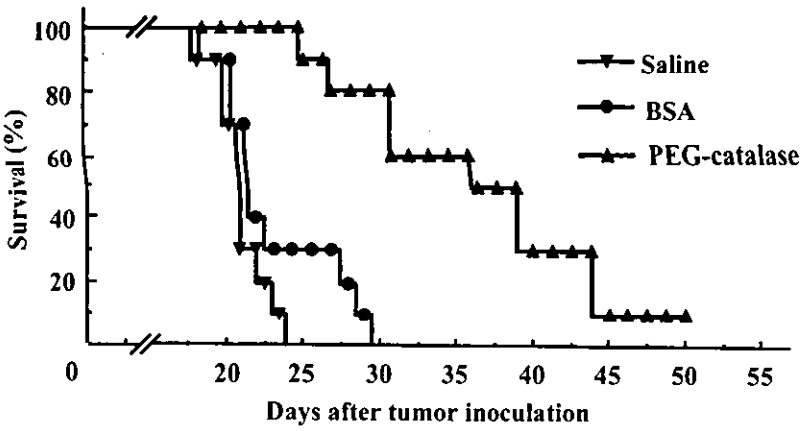

Fig. 6 Survival of mice receiving intravenous injection of B16-BL6cells (1×10^4 cells/mouse). Saline (vehicle), PEG-catalase or BSA was injected daily into the tail vein until 30 days after tumor inoculation. The survival of the PEG-catalase treatment group was significantly longer than that of the saline ($P < 0.0001$) or BSA ($P < 0.01$) treatment group ($n = 10$).

after tumor injection, the injected tumor cells adhere completely to the endothelium and the surviving tumor cells are ready to extravasate and invade the parenchyma of the lung. From day 1 to 3, the tumor cells could have invaded the parenchyma and started to proliferate. An intravital videomicroscopic analysis supports this hypothesis (24).

Even under normal conditions, ROS are continuously produced as by-products of metabolism by enzymes such as superoxide dismutase, xanthine oxidase, and NADPH oxidase (25). Several antitumor drugs as well as radiation also generate ROS through reductive activation and redox recycling (25–27), and it has also been reported that ROS are involved in various processes of tumor metastasis, such as adhesion, invasion and proliferation (5, 6, 9–12). Therefore, the scavenging of ROS by antioxidant enzymes can be an effective approach for inhibiting tumor metastasis. We have proposed a hypothesis that the elimination of H_2O_2 at the site where tumor metastasis occurs reduces this and we have examined the effect of increasing the plasma half-life of catalase on the inhibition of an experimental pulmonary metastasis (8). We found that intravenous injection of PEG-catalase greatly decreased the number of colonies in the lung 2 weeks after tumor injection and, in a separate set of experiments, we have shown that targeted delivery of catalase to hepatocytes greatly inhibited experimental hepatic metastasis in mice (28). These results indicate that the detoxification of H_2O_2 is a promising approach for inhibiting metastasis. However, these results did not identify which metastatic processes are inhibited by the catalase derivatives. To address this question, we measured the number of tumor cells in the lung at 1 hour, 1 and 7 days after injection of tumor cells and examined the effects of catalase derivatives on the metastatic processes.

Administration of PEG-catalase just before tumor injection, which is the same protocol as the one used in a previous study (8), reduced the number of tumor cells in the lung at 24 hours after tumor injection, indicating that PEG-catalase inhibits the early steps of metastasis. Additional studies are needed to identify whether changes in the expression of adhesion molecules are involved in the inhibitory effect of catalase derivatives in the lung. PEG-catalase was effective in reducing the number of tumor cells at day 7, even when intravenously injected at 1 or 3 days after tumor injection. As shown in Fig. 2, the tumor cells in the lung were in a growth phase at the times when PEG-catalase was injected. Therefore, these results indicate that scavenging of H_2O_2 by PEG-catalase can inhibit the growth of metastatic tumor cells. It has already been reported that H_2O_2 can accelerate proliferation (12); therefore, the suppressive effect of catalase derivatives would be attributable to direct inhibition of the proliferation of tumor cells. As shown in Fig. 5*B*, a single injection of PEG-catalase just before tumor injection reduced the number of metastatic nodules but scarcely affected the diameter of the nodules. After triple injection of PEG-catalase (just before, 1 and 3 days after tumor injection), the number of metastatic colonies did not markedly differ from that produced by a single (just before tumor injection) or double (just before and 1 day after tumor injection) injection, although the diameter of the colonies was found to be small. These findings indicate that the first injection of PEG-catalase reduces the number of surviving tumor cells, and the subsequent injections inhibit the proliferation of the surviving tumor cells. Therefore, it is suggested that PEG-catalase inhibits not only the survival or adhesion of tumor cells but also their invasion and proliferation.

Thus, it has been shown that catalase derivatives effectively inhibit not only the early steps of metastasis, but also the later steps. Then, we tried to effectively suppress metastatic tumor growth by inducing tumor dormancy. As shown in Fig. 5*A*, daily injection of PEG-catalase greatly reduced the number of tumor cells detected at 14 days in the lung. The number of tumor cells scarcely increased compared with that detected at 24 hours after tumor injection. Therefore, the tumor cells within the lung tissue may be in a dormant state after repetitive injection of PEG-catalase. This significant inhibition of growth was effective in increasing the survival of the tumor-bearing mice. However, the mice treated with PEG-catalase died sequentially after stopping the injection, suggesting that the tumor cells of micrometastases start to proliferate when the supply of catalase is stopped. In previous publications (29, 30), "dormancy" was used to refer to individual tumor cells that were thought to persist "symbiotically" for long periods, but subsequently could be stimulated to exhibit malignant growth. Therefore, the results of the present study indicate that repeated administration of PEG-catalase can induce tumor dormancy and prolong the survival period.

In conclusion, we have developed a quantitative method to analyze tissue disposition of tumor cells and found that scavenging of H_2O_2 by PEG-catalase can effectively inhibit not only the early steps of metastasis, such as embolization, adhesion, or survival, but also later steps, such as invasion or proliferation. Continuous supply of catalase activity within the blood circulation by multiple dosing of PEG-catalase greatly suppressed the growth of tumor cells in metastatic foci. This reduction of metastatic tumor growth by PEG-catalase offers potentially a very effective approach to the antimetastatic therapy of a variety of tumors.

REFERENCES

1. Engers R, Gabbert HE. Mechanisms of tumor metastasis: cell biological aspects and clinical implications. J Cancer Res Clin Oncol 2000;126:682–92.

2. Zetter BR. The cellular basis of site-specific tumor metastasis. N Engl J Med 1990;322:605–12.

3. Tang DG, Honn KV. Adhesion molecules and tumor metastasis: an update. Invasion Metastasis 14:109–22, 1994.

4. Kannagi R. Carbohydrate-mediated cell adhesion involved in hematogenous metastasis of cancer. Glycoconj J 1997;14:577–84.

5. Onoda JM, Piechocki MP, Honn KV. Radiation-induced increase in expression of the alpha IIb beta 3 integrin in melanoma cells: effects on metastatic potential. Radiat Res 1992;130:281–8.

6. Sellak H, Franzini E, Hakim J, Pasquier C. Reactive oxygen species rapidly increase endothelial ICAM-1 ability to bind neutrophils without detectable upregulation. Blood 1994;83:2669–77.

7. Willam C, Schindler R, Frei U, Eckardt KU. Increases in oxygen tension stimulate expression of ICAM-1 and VCAM-1 on human endothelial cells. Am J Physiol 1999;276:H2044–52.

8. Nishikawa M, Tamada A, Kumai H, Yamashita F, Hashida M. Inhibition of experimental pulmonary metastasis by controlling biodistribution of catalase in mice. Int J Cancer 2002;99:474–9.

9. Shaughnessy SG, Whaley M, Lafrenie RM, Orr FW. Walker 256 tumor cell degradation of extracellular matrices involves a latent gelatinase activated by reactive oxygen species. Arch Biochem Biophys 1993;304:314–21.

10. Rajagopalan S, Meng XP, Ramasamy S, Harrison DG, Galis ZS. Reactive oxygen species produced by macrophage-derived foam cells regulate the activity of vascular matrix metalloproteinases in vitro. Implications for atherosclerotic plaque stability. J Clin Investig 1996; 98:2572–9.

11. Belkhiri A, Richards C, Whaley M, McQueen SA, Orr FW. Increased expression of activated matrix metalloproteinase-2 by human endothelial cells after sublethal H_2O_2 exposure. Lab Investig 1997;77: 533–9.

12. Murrell GA, Francis MJ, Bromley L. Modulation of fibroblast proliferation by oxygen free radicals. Biochem J 1990;265:659–65.

13. Zhang L, Hellstrom KE, Chen L. Luciferase activity as a marker of tumor burden and as an indicator of tumor response to antineoplastic therapy in vivo. Clin Exp Metastasis 1994;12:87–92.

14. El Hilali N, Rubio N, Martinez-Villacampa M, Blanco J. Combined noninvasive imaging and luminometric quantification of luciferase-labeled human prostate tumors and metastases. Lab Investig 2002;82: 1563–71.

15. Edinger M, Sweeney TJ, Tucker AA, Olomu AB, Negrin RS, Contag CH. Noninvasive assessment of tumor cell proliferation in animal models. Neoplasia 1999;1:303–10.

16. Vooijs M, Jonkers J, Lyons S, Berns A. Noninvasive imaging of spontaneous retinoblastoma pathway-dependent tumors in mice. Cancer Res 2002;62:1862–7.

17. Ray P, Wu AM, Gambhir SS. Optical bioluminescence and positron emission tomography imaging of a novel fusion reporter gene in tumor xenografts of living mice. Cancer Res 2003;63:1160–5.

18. Yabe Y, Nishikawa M, Tamada A, Takakura Y, Hashida M. Targeted delivery and improved therapeutic potential of catalase by chemical modification: combination with superoxide dismutase derivatives. J Pharmacol Exp Ther 1999;289:1176–84.

19. Poste G, Doll J, Hart IR, Fidler IJ. In vitro selection of murine B16 melanoma variants with enhanced tissue-invasive properties. Cancer Res 1980;40:1636–44.

20. Nishikawa M, Yamauchi M, Morimoto K, Ishida E, Takakura Y, Hashida M. Hepatocyte-targeted in vivo gene expression by intravenous injection of plasmid DNA complexed with synthetic multi-functional gene delivery system. Gene Ther 2000;7:548–55.

21. Honda M, Kaneko S, Matsushita E, Kobayashi K, Abell GA, Lemon SM. Cell cycle regulation of hepatitis C virus internal ribosomal entry site-directed translation. Gastroenterology 2000;118:152–62.

22. Rubio N, Espana L, Fernandez Y, Blanco J, Sierra A. Metastatic behavior of human breast carcinomas overexpressing the Bcl-x(L) gene: a role in dormancy and organospecificity. Lab Investig 2001;81:725–34.

23. Blood CH, Zetter BR. Tumor interactions with the vasculature: angiogenesis and tumor metastasis. Biochim Biophys Acta 1990;1032: 89–118.

24. Luzzi KJ, MacDonald IC, Schmidt EE, et al. Multistep nature of metastatic inefficiency: dormancy of solitary cells after successful extravasation and limited survival of early micrometastases. Am J Pathol 1998;153:865–73.

25. Warner HR. Superoxide dismutase, aging, and degenerative disease. Free Radic Biol Med 1994;17:249–58.

26. Malisza KL, McIntosh AR, Sveinson SE, Hasinoff BB. Semiquinone free radical formation by daunorubicin aglycone incorporated into the cellular membranes of intact Chinese hamster ovary cells. Free Radic Res 1996;24:9–18.

27. Lazo JS, Sebti SM, Schellens JH. Bleomycin. Cancer Chemother Biol Response Modif 1996;16:39–47.

28. Nishikawa M, Tamada A, Hyoudou K, et al. Inhibition of experimental hepatic metastasis by targeted delivery of catalase in mice. Clin Exp Metastasis. 2004;21:213–21.

29. Hadfield G. The dormant cancer cell. Br Med J 1954;4888:607–10.

30. Fisher B, Fisher ER. Experimental evidence in support of the dormant tumor cell. Science (Wash D C) 1959;130:918–9.

Physicochemical, Tissue Distribution, and Vasodilation Characteristics of Nitrosated Serum Albumin: Delivery of Nitric Oxide *In Vivo*

HIDEMASA KATSUMI,[1] MAKIYA NISHIKAWA,[2] SHEN-FENG MA,[1] FUMIYOSHI YAMASHITA,[1] MITSURU HASHIDA[1]

[1]Departments of Drug Delivery Research. Graduate School of Pharmaceutical Sciences, Kyoto University, Sakyo-ku, Kyoto 606-8501, Japan

[2]Biopharmaceutics and Drug Metabolism, Graduate School of Pharmaceutical Sciences, Kyoto University, Sakyo-ku, Kyoto 606-8501, Japan

Received 2 February 2004; revised 30 April 2004; accepted 4 May 2004

Published online 2 July 2004 in Wiley InterScience (www.interscience.wiley.com). DOI 10.1002/jps.20147

ABSTRACT: Conjugates of nitric oxide (NO) to serum albumins are candidates for controlled delivery of NO *in vivo*, but their physicochemical and tissue distribution characteristics have hardly been examined yet. In this study, to achieve its *in vivo* delivery, bovine serum albumin (BSA) was reacted with sodium nitrite to obtain NO-BSA, which had 0.25–0.28 molecules of S-nitrosothiol/BSA. In addition to cystein, other amino acid residues were modified by the reaction. The conjugation had no significant effect on the molecular weight, but reduced the electric charge and induced reversible changes in the secondary structure of BSA. After intravenous injection in mice at a dose of 1 mg/kg, ^{111}In-NO-BSA slowly disappeared from plasma in a similar manner to ^{111}In-BSA, but showed greater accumulation in the liver and kidney. NO-BSA induced a transient decrease in arterial pressure after intravenous injection in rats at a dose of 100 mg/kg, and significantly increased the distribution of ^{111}In-BSA to the lung in mice. These results indicate that NO is released from NO-BSA shortly after injection, and this NO decreases blood pressure and increases the distribution of macromolecules to the lung. These findings provide useful basic information for designing macromolecular NO donors able to achieve controlled delivery of NO. © 2004 Wiley-Liss, Inc. and the American Pharmacists Association J Pharm Sci 93:2343–2352, 2004

Keywords: conjugation; distribution; macromolecular drug delivery; pharamcokinetics; albumin

INTRODUCTION

Nitric oxide (NO) is involved in a wide variety of physiological and pathological processes. They include vascular smooth muscle relaxation,[1–3] inhibition of platelet aggregation,[4,5] neurotransmission,[6] and immune regulation.[7–9] Because NO elicits protective and beneficial actions in various disease states, NO delivery is expected to be effective in the treatments for essential hypertension, stroke, coronary artery disease, vascular complications of diabetes, erectile dysfunction, and other disorders involving the vascular system.[10] Vasodilation induced by NO would also be useful for improving the permeability of macromolecules across the vascular endothelium, which may solve the delivery problems of associated with genes and proteins.[11]

On the other hand, NO is reported to be cytotoxic in some situations.[12] NO degrades iron-containing prosthetic groups resulting in the inhibition of the mitochondrial respiratory chain and DNA synthesis.[13] NO also reacts with the superoxide anion that is produced by activated

Correspondence to: Mitsuru Hashida (Telephone: +81-75-753-4525; Fax: +81-75-753-4575; E-mail: hashidam@pharm.kyoto-u.ac.jp)

Journal of Pharmaceutical Sciences, Vol. 93, 2343–2352 (2004)

macrophages and other cells, to form peroxynitrite. Its protonated form acts as a potent chemical oxidant,[13] which induces modification of protein functions and DNA damage.[14]

These pieces of evidence suggest that the tissue distribution of NO needs to be well controlled to obtain the therapeutic benefits of NO. Because NO has a very short half life (~0.1 s) *in vivo*,[15] NO donors that generate NO after administration have been developed and used for NO delivery. However, little attention has been paid to the tissue distribution, or controlled delivery of NO *in vivo*. Of the various strategies possible, conjugation of NO to macromolecules appears to be a good approach to control the delivery of NO, because the tissue distribution of the macromolecules can be controlled by various techniques of chemical modification.[16] So far, conjugation of NO to serum albumin or other proteins has been reported,[17,18] and NO-conjugated serum albumin exhibits a number of biological activities of NO such as vasodilation and the inhibition of platelet aggregation. However, their pharmacokinetic properties have been hardly examined so far. It is well known that various kinds of chemically modified proteins are rapidly cleared by scavenging systems in the liver and spleen.[19,20] To control the delivery of NO, the effects of conjugation of NO to the carrier molecule on the tissue distribution of the NO-carrier conjugate should be examined.

In the present study, therefore, we selected bovine serum albumin (BSA, molecular weight of 67,000) as a macromolecular carrier of NO, because serum albumin is an endogenous carrier of NO,[15] and its tissue distribution characteristics are well known. To provide basic information for controlled delivery of NO *in vivo*, we synthesized NO-conjugated BSA (NO-BSA) with various degrees of modification, and analyzed the physicochemical characteristics of NO-BSA such as the apparent molecular weight, electric charge, and the structural characteristics, all of which are determinants of tissue distribution. Then, we examined the tissue distribution of NO-BSA after intravenous injection in mice. Finally, the vasodilating effects of NO-BSA were evaluated in mice and rats after intravenous injection of NO-BSA.

MATERIALS AND METHODS

Animals

Male ddY mice (25–27 g) and male Wistar rats (240–260 g) were purchased from the Shizuoka Agricultural Cooperative Association for Laboratory Animals (Shizuoka, Japan). Animals were maintained under conventional housing conditions. All animal experiments were conducted in accordance with the principles and procedures outlined in the National Institute of Health Guide for the Care and Use of Laboratory Animals. The protocols for animal experiments were approved by the Animal Experimentation Committee of the Graduate School of Pharmaceutical Sciences of Kyoto University.

Chemicals

BSA, sodium nitrite, sulfanilamide and *N*-(1-naphthyl)ethylenediamine dihydrochloride were purchased from Sigma Chemical (St. Louis, MO). Pharmalyte TM 2.5–5 for IEF was purchased from Amersham (Buckinghamshire, England). Amberlyte IRN-150L was purchased from Pharmacia biotech (Uppsala, Sweden). [^{111}In]Indium chloride was supplied by Nihon Medi-Physics (Takarazuka, Japan). Ammonium sulfamate and $HgCl_2$ were purchased from Wako Chemical (Osaka, Japan). All other chemicals were obtained commercially as reagent-grade products.

Synthesis of NO-BSA

NO-BSA with various degrees of modification was synthesized by reacting different amounts of sodium nitrite with BSA as reported previously.[17,18] In brief, BSA (50 mg) and a 200-, 500-, 1000-fold molar excess sodium nitrite was dissolved in 0.5 M HCl. The mixture was stirred for 15 min at 37°C and the reaction terminated by neutralizing the solution at pH 7.5 by the addition of 1 M NaOH and 0.5 M Tris buffer. The products were dialyzed against ultrapure water and concentrated by ultrafiltration at 4°C. UV-visible spectroscopy of NO-BSA was performed with a Beckman spectrometer at a concentration of 2 mg/mL NO-BSA in 0.1 M phosphate buffer at pH 7.4, 25°C. Products were coded as NO(200)-, NO(500)-, and NO(1000)-BSA, according to the molar ratio of sodium nitrite and BSA in the reaction mixture.

Number of NO Adducts on NO-BSA

The number of NO adducts on NO-BSA was determined by Saville assay.[21] In brief, a solution of NO-BSA was mixed with 0.5% ammonium sulfamate in 0.4 M HCl (total volume of 80 μL) for

1 min to remove existing NO_2 and HNO_2 from the solution. Eighty microliters 0.4 M HCl solution containing 3% sulfanilamide and 0.25% $HgCl_2$ was added, followed by the addition of 80 μL 0.1% *N*-(1-naphthyl)ethylenediamine dihydrochloride in 0.4 M HCl. To determine the number of S-nitrosothiol groups on NO-BSA, the mixture was incubated at room temperature for 10 min and the absorbance was read at 540 nm. Separately, to determine the number of total NO adducts on NO-BSA, the mixture was incubated for 5 h at room temperature. The number of NO adducts on NO-BSA was calculated according to a standard curve prepared with 2.5–100 μM $NaNO_2$. The number of free amino groups was determined by trinitrobenzene sulfonic acid using glycine as a standard.[22]

Molecular Weight and Isoelectric Point of NO-BSA

The apparent molecular weight of NO-BSA was estimated by nonreducing SDS-PAGE at 4°C using a standard curve prepared with a set of marker proteins (full range rainbow marker, Amersham, Buckinghamshire, England). The isoelectric point of NO-BSA was determined by isoelectric focusing (NA-1410, Nihon Eidou, Tokyo, Japan) under acidic conditions at 4°C. The gel was composed of acrylamide, bisacrylamide, glycerol, pharmalyte TM 2.5–5 for IEF, amberlyte IRN-150L, TEMED, and ammonium persulfate, and 0.1 M H_2SO_4 and 0.1 M NaOH were used as an anolyte and catholyte, respectively. Samples were applied to the cathode side and subjected to electrophoresis at 100 V for 30 min, 200 V for 30 min, and 400 V for 2 h. The Isoelectric Focusing Calibration Kit (Amersham, Buckinghamshire, England) was used as isoelectric point markers. These assays were performed at 4°C, because NO-BSA is more stable in the solution at low temperature.[17]

Tryptophanyl Fluorescence Spectrum

Intrinsic fluorescence spectra of BSA and NO-BSA were obtained on a RF-540 spectrofluorophotometer (Shimazu, Kyoto, Japan) at 25°C, with a 1-cm quartz cell, thermostatically controlled devices and 10-nm excitation and 5-nm emission bandwidths. BSA and NO-BSA were excited at 295 nm, and the spectra were corrected for buffer baseline fluorescence.

Circular Dichroism (CD) Spectrum

CD spectra of BSA and NO-BSA were measured using a JASCO J-820-type spectropolarimeter (JASCO, Tokyo, Japan) at 25°C. For calculation of the mean residue ellipticity [θ], the molecular weight of BSA and NO-BSA was taken as 67,000. Far-UV and near-UV CD spectra were recorded at protein concentrations of 5 and 15 μM, respectively, in 20 mM sodium phosphate buffer (pH 7.4).

Radiolabeling of BSA and NO-BSA

For the tissue distribution experiments, BSA and NO-BSA were radiolabeled with ^{111}In using the bifunctional chelating agent DTPA anhydride according to the method of Hnatowich et al.[23] In brief, each sample (5 mg) was dissolved in 1 mL 0.1 M HEPES buffer, pH 7, and mixed with two- or threefold molar DTPA anhydride in 10 μL dimethyl sulfoxide. The mixture was stirred for 15 min at room temperature, and the radiolabeled product was purified by gel filtration at 4°C using a Sephadex G-25 column (Pharmacia) to remove unreacted DTPA. The fractions containing the sample were collected and concentrated by ultrafiltration at 4°C. Then, 20 μL $^{111}InCl_3$ solution (37 MBq/mL) was added to 20 μL of 0.1 M citrate buffer, pH 5.5, and 40 μL DTPA-coupled derivative solution was added to the mixture. After 15 min, the mixture was applied to a PD-10 column and eluted with 0.1 M citrate buffer, pH 5.5. The derivative fractions were collected and concentrated by ultrafiltration at 4°C. Radiochemical purity of ^{111}In-BSA and ^{111}In-NO-BSA was confirmed by cellulose acetate electrophoresis, which was run at an electrostatic field of 0.8 mA/cm for 30 min in veronal buffer ($I = 0.06$, pH 8.6). The presence of NO on NO-BSA after radiolabeling was confirmed by the Saville assay as described above.

Tissue Distribution Experiment

Each ^{111}In-NO-BSA was injected into the tail vein of mice at a dose of 1 mg/kg. At appropriate times after injection, blood was collected from the vena cava under ether anesthesia, and the mice were then killed. Heparin sulfate was used as an anticoagulant. Plasma was obtained from the blood by centrifugation. The muscle, liver, kidney, spleen, heart, and lung were removed, rinsed with saline,

and weighed. Urine was also collected. The radioactivity in each sample was counted using a well-type NaI-scintillation counter (ARC-500, Aloka, Tokyo, Japan).

Calculation of Pharmacokinetic Parameter

The ^{111}In radioactivity concentrations in plasma were normalized with respect to the % of the dose/mL and analyzed using the nonlinear least-squares program MULTI.[24] The tissue distribution profiles were evaluated using tissue uptake clearance (CL_{tissue}) according to integration plot analysis. By dividing the amount in a tissue at time t (X_t) and the area under the plasma concentration-time curve (AUC) from time 0 to t (AUC_{0-t}) by the plasma concentration at time t (C_t), CL_{tissue} was obtained from the slope of the plot of X_t/C_t versus AUC_{0-t}/C_t.

Blood Pressure after Intravenous Injection of NO-BSA into Rats

Blood pressure was measured by a strain gauge pressure transducer (P10EZ, Viggo-Spectramed Japan Co., Ltd., Tokyo, Japan) connected to a catheter inserted into the femoral artery of rats. Systolic blood pressure (SBP) and diastolic blood pressure (DBP) before and after the injection of NO(1000)-BSA were recorded every 30 s with a polygraph (poly-Graph 366 system, NEC San-ei Instruments, Co., Ltd., Corporation, Tokyo, Japan), connected to a microcomputer (Dyna-Book J-3100SS, Toshiba Corporation, Tokyo, Japan). NO(1000)-BSA was given by intravenous injection at a dose of 100 mg/kg. Mean arterial blood pressure (MAP) was calculated from SBP and DBP using the following equation:

$$\text{MAP(mmHg)} = (\text{SBP-DBP})/3 + \text{DBP}$$

Effect of NO-BSA on Tissue Distribution of BSA in Mice

The effects of NO-BSA on vascular permeability of macromolecules were evaluated as reported previously [25] with some slight modification. Briefly, ^{111}In-BSA was injected into the tail vein of mice at a dose of 1 mg/kg. At 10 min after injection, NO(1000)-BSA or BSA was injected into the tail vein at a dose of 100 mg/kg. NO(1000)-BSA preincubated for 3 h at 37°C was also used as a control. At 1 min and 5 min after the injection of NO(1000)-BSA or BSA, the blood was collected from the vena cava, then the mice were killed by bleeding. Collecting blood was started at about 5 s before the time indicated, because collecting sufficient volume of blood for analysis takes about 10 s. Then, several tissue samples were collected. The flux of ^{111}In-BSA to tissue was calculated as:

$$\text{Flux} = N/C_P$$

where N is the amount of ^{111}In- BSA in a tissue (expressed as cpm/g tissue) and C_P is the concentration of ^{111}In-BSA in plasma (expressed as cpm/mL blood) at each time point.

RESULTS

Synthesis and Characterization of NO-BSA

The reaction of BSA with sodium nitrite under an acidic conditions produced yellowish solutions with an absorption maximum at 330–350 nm, which is a characteristic of nitrosation products. An absorption peak at 540–545nm, a marker of S-nitrosothiol, was also detected (data not shown). These spectroscopic data were similar to those reported previously.[18]

The number of NO adducts and modified amino groups, apparent molecular weight, and isoelectric point of NO-BSA are summarized in Table 1. The

Table 1. Physicochemical Characteristics of NO-BSA

Compound	Total NO/BSA[a] (mol/mol)	S-NO/BSA[a] (mol/mol)	Molecular Weight[b]	Number of Modified Amino Groups[c] (mol/mol)	Isoelectric Point
BSA	0	0	67,000	0	4.8
NO(200)-BSA	0.70	0.23	67,000	13.4	4.7–4.8
NO(500)-BSA	0.76	0.21	67,000	18.4	4.6–4.7
NO(1000)-BSA	0.79	0.19	67,000	20.5	4.5–4.6

[a]The total NO adducts and S-NO adducts on BSA were estimated by the Saville assay.
[b]The molecular weights of compounds were estimated by nonreducing SDS-PAGE.
[c]The number of modified amino groups were determined by the TNBS method.

total number of NO adducts increased on increasing the concentration of sodium nitrite in the reaction mixture from 0.70 to 0.79. However, the number of S-nitrosothiol groups decreased on increasing in the concentration from 0.23 to 0.19, probably due to the oxidation of thiol.[18,26] Before nitrosation, BSA had 0.38 mol of free SH/mol of protein as determined by the Ellman assay (data not shown), which was consistent with results reported in a previous report.[26] Nitrosation did not significantly alter the apparent molecular weight of any preparation of NO-BSA, whereas the isoelectric point was reduced depending on the degree of chemical modification. The number of modified amino groups increased on increasing the concentration of sodium nitrite from 13 to 21.

Tryptophanyl Fluorescence Spectrum

BSA has two tryptophan residues, one of them being located in an aqueous solvent-exposed environment.[27] We measured the tryptophanyl fluorescence to examine whether the tryptophan residues are nitrosated. As seen in Figure 1, any preparation of NO-BSA had a lower relative fluorescence intensity than BSA. In addition, the λ_{max} was also slightly blue-shifted from 346 to 342 nm. After a 3-h incubation of NO-BSA at 37°C, the fluorescence spectrum of NO-BSA tended to return to that of BSA. These results suggest the possibility that NO bound to the tryptophan residue on BSA is released by incubation, and the structural change produced by modification near the residue is reversible.

CD Spectrum

The secondary structure of BSA and NO-BSA was analyzed by measuring the far-UV CD. The CD spectra of NO(1000)-BSA was slightly shifted compared with that of BSA (Fig. 2). In addition, the near-UV CD spectra of NO(1000)-BSA was also slightly shifted (data not shown). After a 3-h incubation of NO(1000)-BSA at 37°C, both the far-UV and near-UV CD spectra of NO(1000)-BSA became closer to those of BSA.

Distribution of ^{111}In-NO-BSA after Intravenous Injection in Mice

Figure 3 shows the time courses of the concentrations in plasma and the liver and kidney concentrations of ^{111}In-radioactivity after intravenous injection of ^{111}In-BSA or ^{111}In-NO-BSA in mice at a dose of 1 mg/kg. As reported previously, ^{111}In-BSA slowly disappeared from the blood circulation. ^{111}In-NO(200)-BSA, ^{111}In-NO(500)-BSA, and ^{111}In-NO(1000)-BSA also slowly disappeared from the blood circulation in a similar manner to ^{111}In-BSA. However, all ^{111}In-NO-BSAs showed greater accumulation in the liver and kidney during the first hour after injection; the amounts of radioactivity recovered in the liver were 0.6 ±

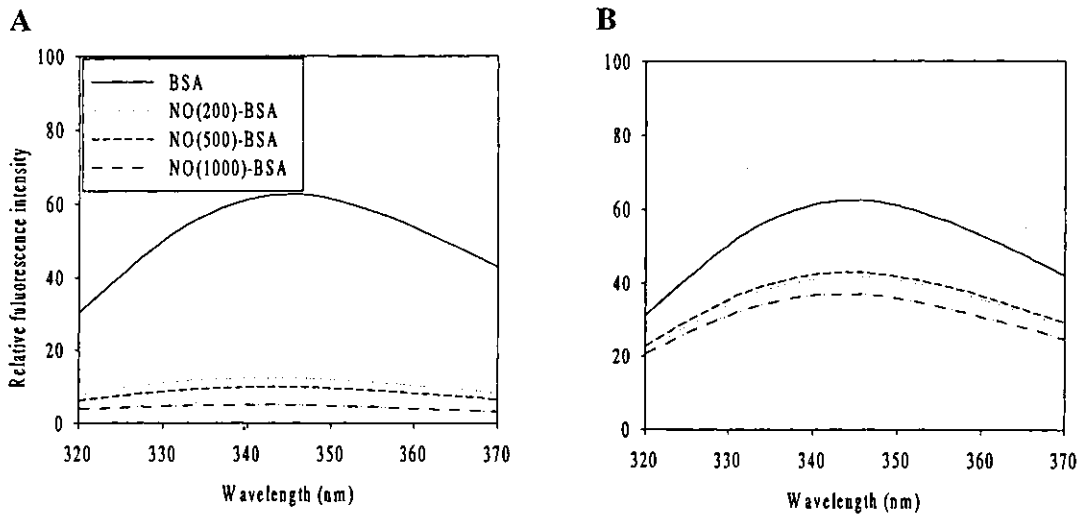

Figure 1. Intrinsic fluorescence spectra of BSA and NO-BSA at 25°C. Each sample solution (2 μM in 0.1 M sodium phosphate buffer, pH 7.4) was excited at 295 nm and the emission fluorescence was detected from 320 to 370 nm. (A) protein without incubation; (B) protein incubated for 3 h at 37°C.